Chemical Engineering Journal 506 (2025) 159965

Contents lists available at ScienceDirect

Chemical Engineering Journal

journal homepage: www.elsevier.com/locate/cej

Competitive adsorption-penetration characteristics of multi-component gases in micro-nano pore of coal

Honggao Xie [a,b], Shuxun Sang [a,b,c,d,*], Xijian Li [e], Zhihua Yan [a,f], Xiaozhi Zhou [a,b], Shiqi Liu [c,d], Sijie Han [c,d], Junjie Cai [e]

[a] School of Resources and Geosciences, China University of Mining and Technology, Xuzhou 221116 China
[b] Key Laboratory of Coalbed Methane Resources and Reservior Formation Process, Ministry of Education, China University of Mining and Technology, Xuzhou 221116 China
[c] Carbon Neutrality Institute, China University of Mining and Technology, Xuzhou 221008 China
[d] Jiangsu Key Laboratory of Coal-based Greenhouse Gas Control and Utilization, China University of Mining and Technology, Xuzhou 221008 China
[e] College of Mining, Guizhou University, Guiyang 550025 China
[f] Guizhou Research Center of Shale Gas and CBM Engineering Technology, Guiyang 550081 China

ARTICLE INFO

Keywords:
Coalbed methane
Multi-component gases
Micro-nano pore
Pore structure parameters
Competitive adsorption-diffusion

ABSTRACT

Clarifying the competitive adsorption-diffusion mechanism of multi-component gases (CH_4, CO_2, N_2) in micro-nano pores is essential for efficiently developing coalbed methane (CBM) resources. This paper reveals the relationship between pore structure parameters—fractal dimension (D_m, D_1, D_2, D), average pore-throat ratio (P_t), anisotropy ($A_{ave,total}$) and accessibility (χ) of micro-nano pores—and adsorption capacity and diffusion coefficient of multicomponent gases. The results show that P_t, $A_{ave,total}$ and χ are positively correlated with D_m, D_2 and D, and negatively correlated with D_1. When $D_m > 2.05$, The total adsorption capacity of multi-component gas at penetration, dry, and equilibrium points increases significantly with the increase of D_m of micropores. The total adsorption capacity of multi-component gas declines as D_1 rises, while it improves with the elevation of D_2 and D, though the rate of improvement is slow. The adsorption capacity of multi-component gas increases with the increase of average vitrinite reflectance ($\overline{R}_0$>1.8 %), $A_{ave,total}$ and χ. The adsorption capacity of the three gases is $CO_2 > CH_4 > N_2$, the diffusion capacity is $N_2 > CH_4 > CO_2$, while the sequence of mass transfer zone length is $CH_4 > CO_2 > N_2$. The diffusion coefficient of multi-component gas increases with higher values of D_m and D_1, but falls as $\overline{R}_0$ and $A_{ave,total}$ grow. In coal with a high metamorphic degree, developed matrix pores result in greater pore heterogeneity, which lowers gas diffusion efficiency. The research findings have considerable importance for the adsorption-diffusion of multi-component gases and the enhancement of CBM production.

1. Introduction

As coal resources are mined to greater depths, the three attributes of coalbed methane (CBM)—as an energy gas, disaster gas, and greenhouse gas—are becoming increasingly prominent. Since the 1980 s, CBM is considered a clean energy source and has developed into a significant unconventional natural gas resource[1]. Gas pressure is a crucial factor for coal and gas protrusion in coal mines, and reducing gas pressure through surface-underground gas extraction can effectively mitigate the risk of gas protrusion[2,3]. CBM is a major sources of greenhouse gas emissions and has a greenhouse effect that is 28 times greater than that of carbon dioxide by volume[4,5]. In the context of global methane emission reduction, for China, which is "rich in coal, poor in oil, and poor in gas", the development of CBM is significant in alleviating the shortage of natural gas resources, reducing the hazards of gas, and lowering methane emissions[6–8]. However, efficient CBM extraction requires breakthroughs in engineering bottlenecks, precise delineation of the pore and fracture structure of coal reservoirs, and elucidation of the rules governing CBM desorption and transport to address the challenges of extracting low-permeability coal seams.

CBM development is a multi-scale scientific research problem that combines macro and micro aspects. In the past, Scholars have studied the engineering aspects of CBM development, concentrating on extraction methods[9]. For high gas content coal seams with low-ultra-low

* Corresponding author at: School of Resources and Geosciences, China University of Mining and Technology, Xuzhou 221116, China.
E-mail address: shxsang@cumt.edu.cn (S. Sang).

https://doi.org/10.1016/j.cej.2025.159965
Received 4 December 2024; Received in revised form 22 January 2025; Accepted 24 January 2025
Available online 30 January 2025

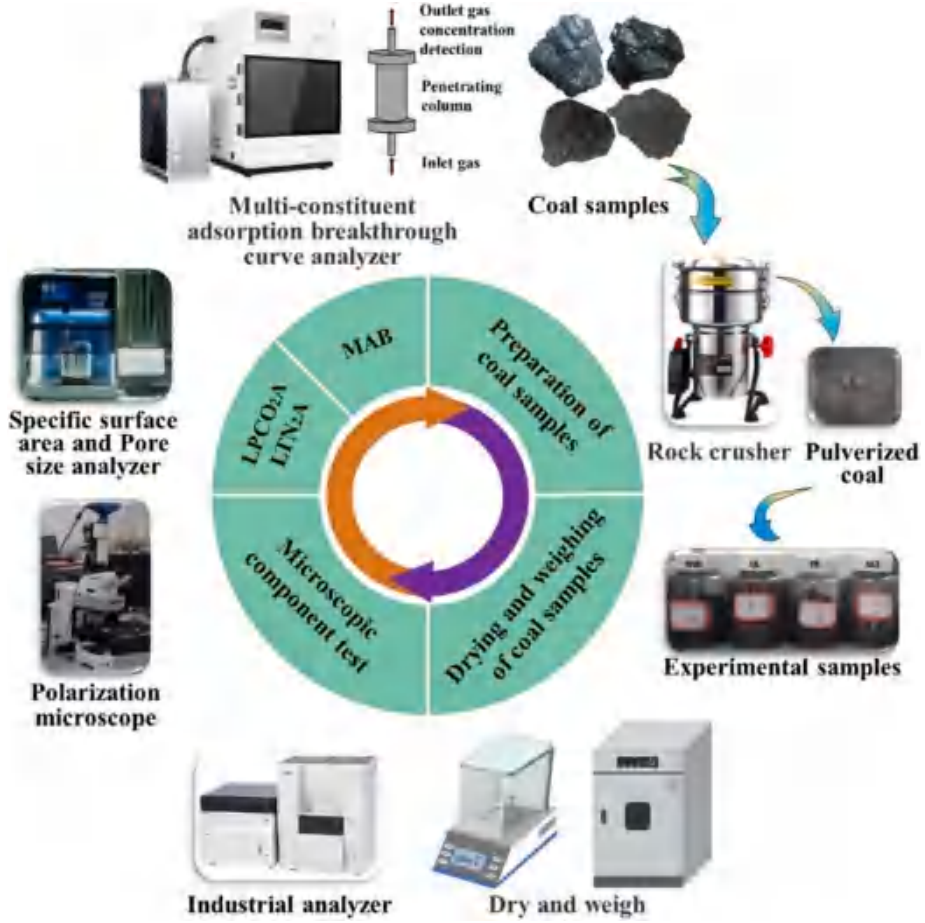

Fig. 1. Experimental equipment and experimental process.

permeability, accurately characterizing the reservoir and increasing permeability through reservoir modification processes has become an important research area for enhancing CBM production[10–12]. Currently, "fracture stimulation – hydrophobic pressure reduction – desorption and gas extraction" is the commonly used approach for CBM development, but for tectonic coal (soft and low-permeability) reservoirs, "stress release – expansion and pressure reduction – desorption and permeability enhancement and gas extraction" has been proposed as the path for CBM development[13]. Methane desorption and transport in the pore-fracture network in the above two models are key to efficient CBM extraction [14,15]. Therefore, the adsorption/desorption-transport of CBM in porous media and other fine-scale microscopic scientific problems have become hotspots for many scholars.

The fine-scale microscopic aspects of CBM development include the microstructure of coal, pore and fracture structure, molecular structure, and the status of gas storage in coal. Most of the CBM is stored in the coal beds in the adsorption state, with the composition of CBM dominated by CH_4, containing N_2, CO_2, H_2S, and other gases[16,17]. The key to the efficient development of CBM lies in elucidating the structural characteristics of coal reservoirs and the mechanisms of gas transport and enrichment, which involves the characterization of the micro-components, chemical components, molecular structure, and porous structure of the coal, as well as the adsorption, desorption, diffusion, and permeability of the gas[18–24]. Researchers have conducted molecular simulations, laboratory tests, and theoretical model analyses of pore connectivity and single-component gases in pore fissures in coal or shale to examine the effects of water content, temperature, pressure, and pore nano-limited domain effects on gas transport mechanisms[25–28]. Some scholars studied the competitive adsorption capacity of CO_2 and CH_4 in different pore diameters using molecular simulation, and concluded that the adsorption capacity of CO_2 increased with increasing pore diameter, or studied the competitive adsorption of binary mixture of CO_2 and CH_4 using experiments, and perfected the effect of the gas ratios on the competitive adsorption capacity[29–31]. Others have discussed the effects of pressure, temperature, coal particle size, and N/S elements in coal on the competitive adsorption and diffusion characteristics of CH_4, CO_2, and N_2 gases, thereby deepening the understanding of the mechanisms associated with competitive gas adsorption in coal[32,33]. However, the relationship between the structural properties of micro-nano pore fractures (including fractal features, anisotropy, and accessibility) and the competitive adsorption-penetration characteristics of multi-component gases (CH_4, CO_2, and N_2) in coal has rarely been reported. Therefore, the study of the structural characteristics of micro-nano pores and the competitive adsorption-penetration characteristics of gases in coal in this paper will positively impact the assessment of the ease or difficulty of CBM transport in micro-nano pores.

In this study, the microstructural characteristics of coal samples were investigated using coal rock microanalysis, low-pressure CO_2 adsorption ($LPCO_2A$), and low-temperature N_2 adsorption (LTN_2A) tests. The micro-nano pores structural characteristics of coal, along with the challenges of gas adsorption and migration, were analyzed based on fractal theory, pore-throat ratio, anisotropy, and accessibility. The adsorption and diffusion parameters of the multicomponent gases (CH_4, CO_2, and N_2) were obtained from multicomponent gas competitive adsorption-penetration curve experiments. Additionally, the relationship between these characteristics and the gas adsorption-diffusion properties was revealed in conjunction with the micro- and nanopore structure of coal. This study holds great theoretical significance for elucidating the transport of multicomponent gases and methane production through CO_2/N_2 gas displacement in CBM mining.

2. Experiments and methods

To realize large-scale CBM development, the gas adsorption, desorption, diffusion, and seepage laws in difficult-to-desorb coal seams must be clarified, and the gas desorption-diffusion mechanism of CH_4, CO_2, and N_2 in micro-nanopores is crucial for increasing CBM production. In this study, the relationship between competitive adsorption-diffusion of multicomponent gases in micro- nano pores is investigated using micro- nano pore parameters, such as fractal dimension, pore-throat ratio (P_t), anisotropy ($A_{ave,total}$) and accessibility(χ), aiming to elucidate in depth the competitive adsorption-transport law of multi-component gases in the process of CBM development.

2.1. Samples and experimental procedures

Coal samples were collected from the tectonic coal sections of the Wenjiaba (WJB), Qinglong (QL), and Faer (FR) coal mines in western Guizhou Province. These coal samples were subjected to tectonic effects, and the DLT sample was taken from the primary structural coal of the Daliuta (DLT) coal mine in Shenmu City, Shaanxi Province. The experimental process is illustrated in Fig. 1. The fresh coal samples were transported to the laboratory in sealed containers, crushed using a coal rock crusher, screened to a particle size 20 mesh (0.85 mm), 100 mesh (0.15 mm), and 60–80 mesh (0.18 mm–0.25 mm), then dried. Subsequently, they were loaded into specimen bottles for sealed preservation. Experiments on coal rock components, micro- and nano-pore characterization of coal ($LPCO_2A$ and LTN_2A), and adsorption-penetration curves of multi-component gases of coal were conducted.

2.2. Characterization methods of coal components and micro-nano pores

Coal microcomponent and vitrinite reflectivity test using the Axiao scope A1 Zeiss microscope produced by Zeiss, Oberkochen, Germany, under the 50 times objective lens, the vitrinite, inertinite and exinite were identified and counted, respectively. At least 500 effective points to be identified and counted, and then according to the number of effective points of each component to calculate its corresponding percentage content. At the same time, the vitrinite reflectivity was counted using MSP200 software, and WS-G818 full-automatic industrial analyzer produced by Changsha YG-WILLSULL, China, was used to test the conventional components in coal.

The $LPCO_2A$ test utilized ASAP2460 fully automated specific surface area and pore size analyzer produced by Micromeritics, USA, with a relative pressure of 0–0.03 to conduct CO_2 adsorption/desorption experiments at an absolute temperature of 273.15 K. Because CO_2 has a higher density and pressure at saturation temperatures, it is capable of testing micropores smaller than 2 nm in coal. The density function theory (DFT) model was used to obtain the experimental micro-pore data of $LPCO_2A$ (This is abbreviated as CO_2-DFT). The LTN_2A test employed a BSD-660 fully automated high-throughput specific surface area and pore size analyzer produced by Beishide Instrument-S&T. (Beijing) Co., Ltd., China, with a relative pressure of 0–0.998. N_2 adsorption/desorption experiments were performed at 77.3 K, Mesopore and macrospore (2 nm–200 nm) data were obtained by Barrett-Joyner-Halenda (N_2-BJH), mesopore (2 nm–50 nm) data were obtained by N_2-DFT model, 0.36 nm^{-1} nm pore data can be obtained by T-polt model (Created by Lippins, Linsen and De Boer), and 1 nm^{-2} nm pore data were calculated by Horvath-Kawazoe (HK) model.

2.2.1. Pore fractal model

Probe molecules of various diameters can access different pore spaces, typically using CO_2 for pores smaller than 2 nm and N_2 for pores ranging from 2 to 200 nm, to characterize their fractal features. Zhang and Li [34], Wang and Li [35] analyzed the correlation between CO_2 adsorption capacity and relative pressure (μ=P/P_0) and concluded that Eq. (1) below can describe the surface fractal law of micropores.

$$\ln\omega(\mu) = C + D_m \ln\beta(\mu) \tag{1}$$

where, D_m is the fractal dimension of the microporous surface, C is a constant term,$\omega(\mu) = \frac{\int_{N(\mu)}^{N_{max}} \ln(\mu) dN(\mu)}{r(\mu)^2}$, $\beta(\mu) = \frac{(N_{max} - N(\mu))^{\frac{1}{3}}}{r(\mu)}$, where N_{max} represents the adsorbed amount at the maximum relative pressure, cm^3/g, the pore space covered by CO_2 varies at different pressure stages, and the relationship between r and the relative pressure is characterized by Kelvin's Eq. (2):

$$r = \frac{2\sigma\nu}{RT(-\ln\mu)} \tag{2}$$

where, σ represents the surface tension; ν is molar volume, 22.4 L/mol; R signifies the ideal gas constant, 8.314 J/(mol·K). T denotes the absolute temperature, K.

LTN_2A adsorption data-derived fractal dimensions emerged as an effective method for characterizing pore geometries in porous media, quantitatively pore surface roughness(D_1) and pore structure(D_2) [24,36,37]. Based on the Frenkel-Halsey-Hill (FHH) model, Eq. (3) facilitates the calculation of the fractal dimension [38].

$$\ln\left(\frac{V}{V_0}\right) = C + (D-3)\ln\left[\ln\left(\frac{P_0}{P}\right)\right] \tag{3}$$

where, the value of D is usually between 2 and 3.

2.2.2. Average pore throat ratio and anisotropy

It is assumed that the pore space in coal consists of M similar cylindrical pores with local pore length L, mean pore radius r, and local anisotropy ($B = L/r$). The average pore diameter (D_{ave}) of a porous material is a commonly used pore parameter, which in terms of pore volume and specific surface area consists of an ensemble of M identical cylindrical pores with a length of L and a diameter of d. In this study, the pore volume and specific surface area data were obtained by physical adsorption method to solve the relationship between the D_{ave}, and the pore volume(V), and specific surface area(A), with the Eq. (4):

$$\frac{V}{A} = \frac{M\pi(D_{ave}/2)^2 L}{M{\cdot}2\pi(D_{ave}/2)L} = D_{ave}/4 \tag{4}$$

The expression for D_{ave} versus V and S is Eq. (5):

$$D_{ave} = \frac{4000V}{S} \tag{5}$$

The P_t with the average radius of mesopores ($r_{1,ave}$), and the average radius of macropores ($r_{2,ave}$) are expressed by the following Eq. (6):

$$P_t = \frac{r_{2,ave}}{r_{1,ave}} = \frac{V_{2,BJH}A_{1,BJH}}{A_{2,BJH}V_{1,BJH}} \tag{6}$$

where $V_{1,BJH}$ is the mesopore pore volume, cc/g; $A_{1,BJH}$ represents the mesopore specific surface area, m^2/g; $V_{2,BJH}$ represents the macropore pore volume, cc/g; $A_{2,BJH}$ is the macropore specific surface area, m^2/g.

Margellou et al[39]. Zipf's rule for calculating the nanoscale $A_{ave,total}$ of porous media materials yields that the $A_{ave,total}$ can be characterized by the pore volume versus the specific surface area. In this section, the anisotropy of the total average pore structure of coal ($A_{ave,total}$) is explored using the BJH model data in LTN_2A. The anisotropy per gram of coal can be obtained from the ratio of the total pore length L_{total} to the total average pore diameter D_{ave}, as shown in Eq. (7):

$$A_{ave,total} = \frac{L_{total}}{D_{ave}} \tag{7}$$

where $A_{ave,total}$ is the total average $A_{ave,total}$ per unit (per gram) mass of coal, g^{-1}; and L_{total} denotes the total pore length, nm/g. After unification of the units, L_{total} can be calculated from the total pore volume and the total specific area with the expression:

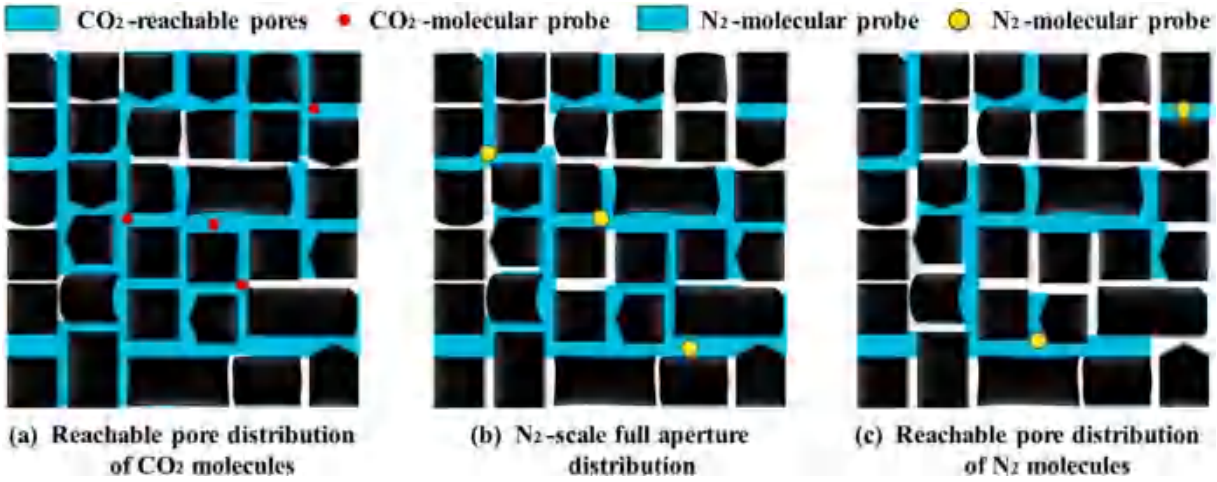

Fig. 2. Accessibility of simplified pore structure utilizing percolation theory.

$$L_{total} = \frac{10^{15}}{4\pi} \cdot \frac{A_{BJH}^2}{V_{BJH}} \tag{8}$$

2.2.3. Pore accessibility

The phenomenon of hysteresis loops observed in the experimental adsorption/desorption curves of LPCO$_2$A and LTN$_2$A is intimately tied to the pore's morphological structure. To gain a deeper understanding and practical application of microscopic pore *accessibility* (χ) and its connectivity effects on gas molecule transport, this section introduces the percolation theory to explore the χ of the simplified coal [40].

The core of the percolation theory is that when the porosity of contracted pores in coal reaches a specific value, gas molecules within the pore system have a higher probability of being transported from the inside out. In this paper, two different probes, CO_2 and N_2, are selected to characterise the pore variability. The kinetic diameter of CO_2 is 0.33 nm, and the CO_2-DFT pore size distribution of the coals from the four mining areas can be assumed to be the full-scale pore size distribution of the microporous stage f_a(r); whereas, the N_2 molecules can be involved as adsorbate molecules in the adsorption under the condition of liquid nitrogen, and the pore size distribution of the N_2-DFT will be as the pore size distribution f_b(r) of N_2 molecules up to the pore scale [41]. Fig. 2 shows the schematic diagrams of CO_2 and N_2 molecular probes transported within the simplified pore structure, respectively. Fig. 2(a) shows the CO_2 molecular reachable pore distribution, i.e., f_a(r); Fig. 2(b) shows all the pore channels that allow the N_2 molecular transport without considering the connectivity condition, with the probability of G_1. Fig. 2 (c) shows the N_2 molecular reachable pore distribution with the probability of G_2, with considering the connectivity condition. under the assumption that the pore structure parameters are independent of pore size, G_1 can be solved by CO_2 adsorption pore size distribution with the following Eq.(9):

$$G_1 = \frac{\int_{r_{N_2,\min}}^{r_{\max}} \frac{f_a(r)}{r} dr}{\int_{r_{\min}}^{r_{\max}} \frac{f_a(r)}{r} dr} \tag{9}$$

where r_{max} and r_{min} represent the maximum and minimum pore sizes, respectively, determined by CO_2-DFT, with values of 1.1 nm and 0.36 nm. Additionally, $r_{N2,\min}$ denotes the minimum pore size derived from N_2-DFT, which is taken as 0.8 nm. The G_2 represented in Fig. 2(c) can be expressed by the distribution of the pore sizes of the CO_2-N_2 adsorption, with the following Eq. (10):

$$G_2 = \frac{\int_{r_{N_2,\min}}^{r_{\max}} \frac{f_b(r)}{r} dr}{\int_{r_{\min}}^{r_{\max}} \frac{f_a(r)}{r} dr} \tag{10}$$

According to the accessibility analysis of previous scholars based on the molecular dynamics cubic lattice structure, G_1 and G_2 obey the following relationship without considering the pore connectivity[42]:

$$\begin{gathered} \chi G_2 = 0, \chi G_1 < 1.494 \\ \chi G_2 = 1.1314(\chi G_1 - 1.494)^{0.41} + 3.153(\chi G_1 - 1.494) \\ -3.48(\chi G_1 - 1.494)^2 + 1.433(\chi G_1 - 1.494)^3, 1.494 < \chi G_1 < 2.7 \\ \chi G_2 = \chi G_1, \chi G_1 > 2.7 \end{gathered} \tag{11}$$

where χ is the accessibility coefficient, which can indicate the overall accessibility magnitude of the porous medium.

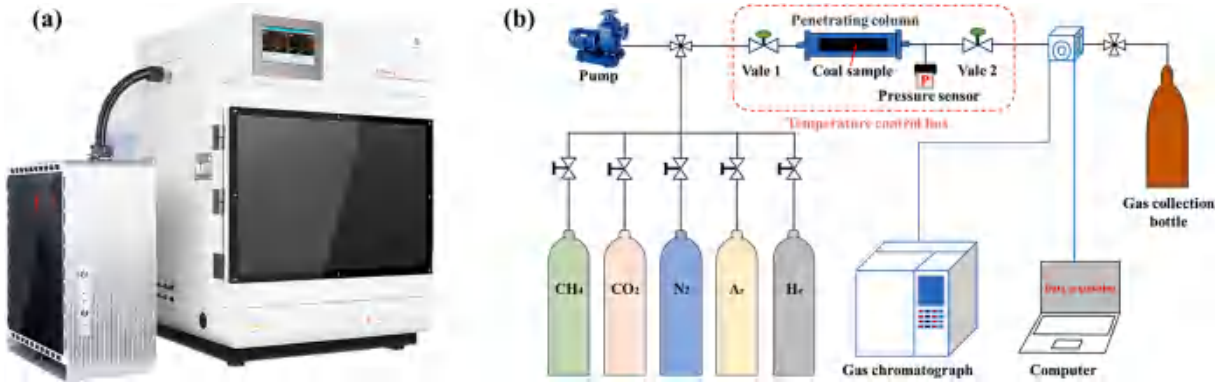

Fig. 3. Multi-component competitive adsorption-permeation curve analyzer and operating schematic: (a) BSD-MAB instrumentation and (b) schematic of the operating principle.

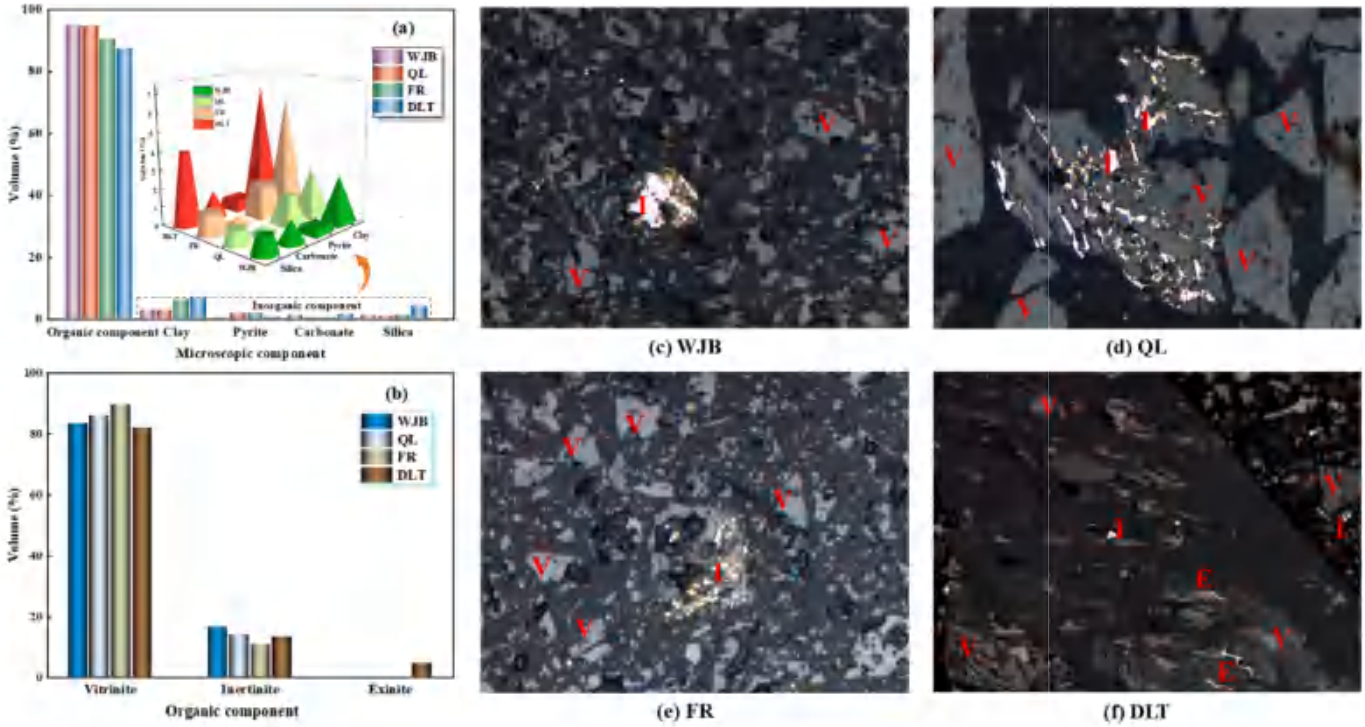

Fig. 4. Microcomposition of coal: a–b, contents of mineral and organic components; c–f, maceral image of coal. Note: V is Vitrinite, I is Inertinite, E is Exinite.

2.3. Multi-component gas adsorption-penetration experiments

This paper conducted a room-temperature (25 °C) to study coal's multicomponent gas competitive adsorption-penetration characteristics. The instrument used for the experiment was the BSD-MAB multicomponent competitive adsorption-penetration curve analyser produced by Beishide Instrument-S&T. (Beijing) Co., Ltd., China (Fig. 3a). The instrument consists of a gas supply system, a vacuum system, an adsorption system, a gas flow control system and a detection system. A brief schematic of the operation of the apparatus is shown in Fig. 3b. The experimental steps are as follows: Firstly, the sample of coal dust (60–80 mesh) was activated and heated and purged under inert gas (He) for 2 h. Then, the adsorption parameters were set to be 10.0 mm in inner diameter of the penetration column, 25 ℃ in testing temperature, 101.0 KPa in pre-column and post-column pressures, and 10 mL in free space of the column, with the loading length of the sample being not less than 10 cm. The volumetric percentage of CH_4 in the CBM was about 80 %, and therefore The volume-percentage concentration ratio of each component gas was set to be CH_4: N_2: CO_2 = 8:1:1, and the adsorption-penetration test was carried out under the condition of Ar as the reference gas.

To investigate the competitive adsorption law of multi-component gases, Eq. (12) was used to examine the adsorption capacity of coal for CH_4, N_2, and CO_2 [43].

$$Q = \frac{1}{M}\int_0^t F\left(C_0 - \frac{1-C_0}{1-C_i}C_i\right)dt \tag{12}$$

where Q denotes the gas adsorption volume, mL/g; M is the mass of adsorbent in the penetrating column, g; F is the inlet gas flow rate, mL/min; C_0 and C_i are the concentration of the outlet gas and the concentration of the inlet gas at time t, V/V %.

The diffusion coefficient, which is crucial for measuring gas transport within a coal reservoir[44], In the penetration experiment, the process of gas passing through the coal sample can be regarded as a one-dimensional diffusion process. According to the diffusion theory, the diffusion rate is proportional to the diffusion coefficient D_f and can be described by Fick's law. Under steady state conditions, the diffusion distance L versus time t can be expressed by the following Eq. (13):

$$L = \sqrt{D \cdot t} \tag{13}$$

Based on Eq. (13), the above equation can be rewritten by considering the delay time t_{eq}:

$$L^2 = D \cdot t_{eq} \tag{14}$$

By replacing D with D_f, the Eq. (15) is obtained:

$$D_f = \frac{L^2}{t_{eq}} \tag{15}$$

where D_f is the effective diffusion coefficient, cm^2/s; L is the length of the loaded sample and the thickness of the penetration column, cm; and t_{eq} is the delay time, s.

The formula for the diffusion coefficient D_f reflects the basic characteristics of gas transport within coal reservoirs, and the diffusion capacity of gases in coal seams can be effectively assessed through the relationship between the loading length L and the delay time t_{eq}.

3. Results

Coal reservoir methane yield capacity is related to matrix pore methane desorption capacity, methane organic matter pore-to-fracture network diffusion conditions and other factors. This paper mainly analyses the connectivity characteristics of micro-nano pores and fractures in coal from the perspective of pore-fracture morphological features (pore fractal characteristics, P_t, $A_{ave,\ total}$, and χ).

Table 1
Proximate analysis and vitrinite reflectivity of coal.

Sample number	Proximate analysis (%)					R_O	$\overline{R}_0$(%)
	M_{ad}	V_{ad}	A_{ad}	FC_d	V_{daf}		
WJB	0.76	6.85	6.32	86.07	8.67	3.38–3.93	3.65
QL	1.35	6.21	7.12	85.32	6.78	2.85–3.48	3.17
FR	1.12	14.36	17.45	67.07	17.63	1.58–2.09	1.81
DLT	2.49	29.28	17.87	50.36	34.92	0.50–0.78	0.63

3.1. Microcomposition and micro- and nanopore analysis of coal

3.1.1. Component and microscopic characterisation of coal

The theory of coal petrography divides the organic matter in coal into three types: vitrinite, inertinite and exinite, and the exinite has a low reflectivity in coal, which is difficult to be recognised under oil immersion reflected light. Under the reflected light oil immersion microscope, the vitrinite and inertinite were generally observed in the tested coal samples. However, only a small amount of exinite was observed in the DLT, and the exinite was not particularly prominent in the other coal samples. The results of the microscopic composition analysis of the coal are shown in Fig. 4.

By examining the mineral and microscopic components of the coal, it is evident that the proportion of organic matter components in the sample is 87.4 %~94.8 %, clay minerals are 2.6–6.6 %, pyrite minerals are 0.4–2.17 %, carbonate minerals are 0.4–1.4 %, and quartz is 0.8–4 %. Among these, DLT coal samples contain the highest mineral content and the highest proportion of clay minerals. the study shows that the proportion of the vitrinite fraction in the specimen's organic matter is 82.11–92.54 %, the proportion of the inertinite is 7.46–16.5 %, and only the DLT sample has an exinite fraction of 4.59 %. According to the content of the specular group, it can be concluded that the test coal samples are all high specular group coals.

The industrial analyses of the coals and the reflectance results of the specular mass group are shown in Table 1. Combined with the ash output of the coals, the DLT specimen is a medium-ash coal, and the rest of the coals belong to lower-ash coals. Based on the industrial analysis, microcomponent analysis and mirror group reflectivity results of the coals, it can be concluded that the QL and WJB specimens are low ash-high mirror group-high coal rank coals I, and the FR coals are lower ash-high mirror group-medium coal rank VII. The DLT is medium ash-high mirror group-medium coal rank I. Specifically, DLT is a gas coal, FR is a poor coal, and WJB and QL are anthracite coals. The order of coaling degree and organic matter content from high to low is WJB, QL, FR and DLT. The study also reveals that coal samples with a high degree of coalification exhibit more prominent organic matter pores, featuring diverse pore morphologies. Additionally, these samples contain a higher composition of clay minerals (as shown in Fig. 4), which are factors influencing the storage and production of CBM.

3.1.2. Analysis of micro-nano pore structure distribution of coal

Coal is a complex porous medium whose morpho-physical structural features control gas transport, and the focus of determining transport modes and pathways is on coal matrix pore connectivity and geometric features (slit-type pores, ink-bottle pores, wedge-type pores, and cylindrical shapes, etc.)[45,46]. Among the many methods of pore characterisation, the fluid intrusion method, based on pressed mercury and physical adsorption, is the most common to study complex pores [47–49]. In this research, CO_2 and N_2 were used as probes to study the morphological characteristics of pore structure at the nano-micron scale in coal.

The maximum adsorption amount of CO_2 is WJB, FR, QL and DLT in descending order, and the maximum adsorption amount of N_2 is WJB, DLT, QL and FR in descending order (see Fig. 5). The micropores of WJB coal samples are more developed, so it is easier to enter the molecules of CO_2 and N_2, and the adsorbed amount of the gases is increased. DLT sample is a low-rank coal bituminous coal, not as compact as anthracite, the primary microporosity pore is more developed, and thus the CO_2 and N_2 are easier to enter. The hysteresis loops between the CO_2/N_2 adsorption–desorption curves in the samples and the non-closure of the adsorption–desorption curves indicate that there are pores similar to the shape of "ink bottles" in the samples, which make it difficult to desorb the gases after adsorption.

In this paper, we utilized the IUPAC pore classification system to categorize the pores in the specimens into three types: micropores (with diameters less than 2 nm), mesopores (ranging from 2 to 50 nm), and macropores (exceeding 50 nm in diameter)[50]. The DFT model is often used to study micropores in LPCO$_2$A experiments to obtain the pore size distribution and pore parameters of micropores (0.36 nm–1.1 nm) that can be reached by CO_2 molecules smaller than 2 nm; the N_2-BJH model is used to study mesopores and macropores, and the N_2-DFT model is used to assist in the study of mesopore pore size distributions in coals with less than 50 nm pores. The pore size distributions for pores smaller than 50 nm were in the order of WJB, DLT, QL and FR (See Fig. 6). According to the LTN$_2$A experiment, the most available pore sizes of WJB, QL, FR and DLT are 1.8002 nm, 2.0342 nm, 2.1796 nm and

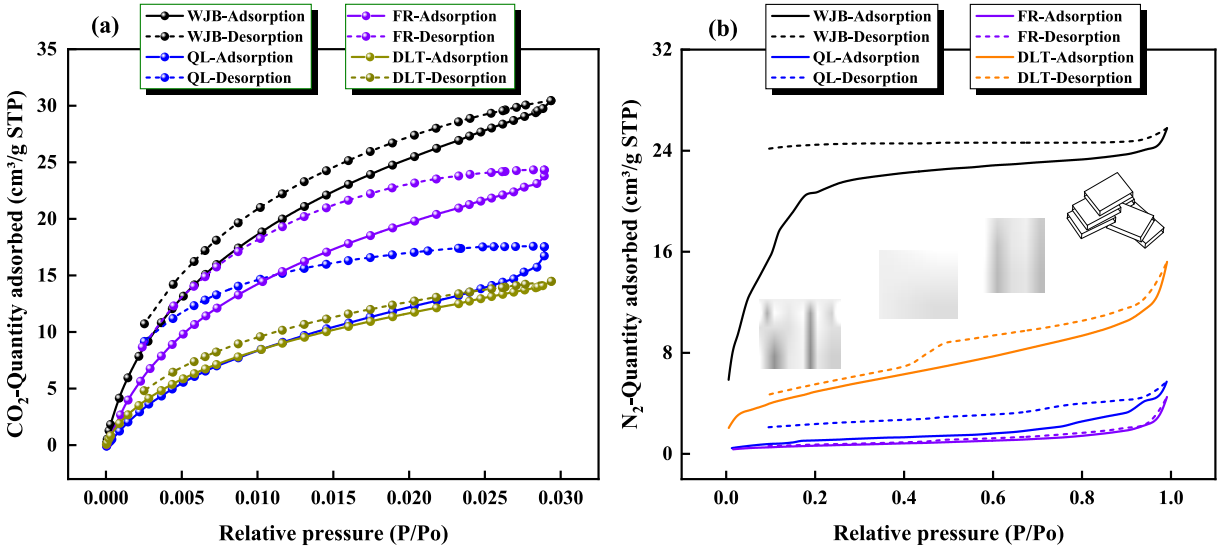

Fig. 5. Adsorption-desorption curves of (a) LPCO$_2$A and (b) LTN$_2$A.

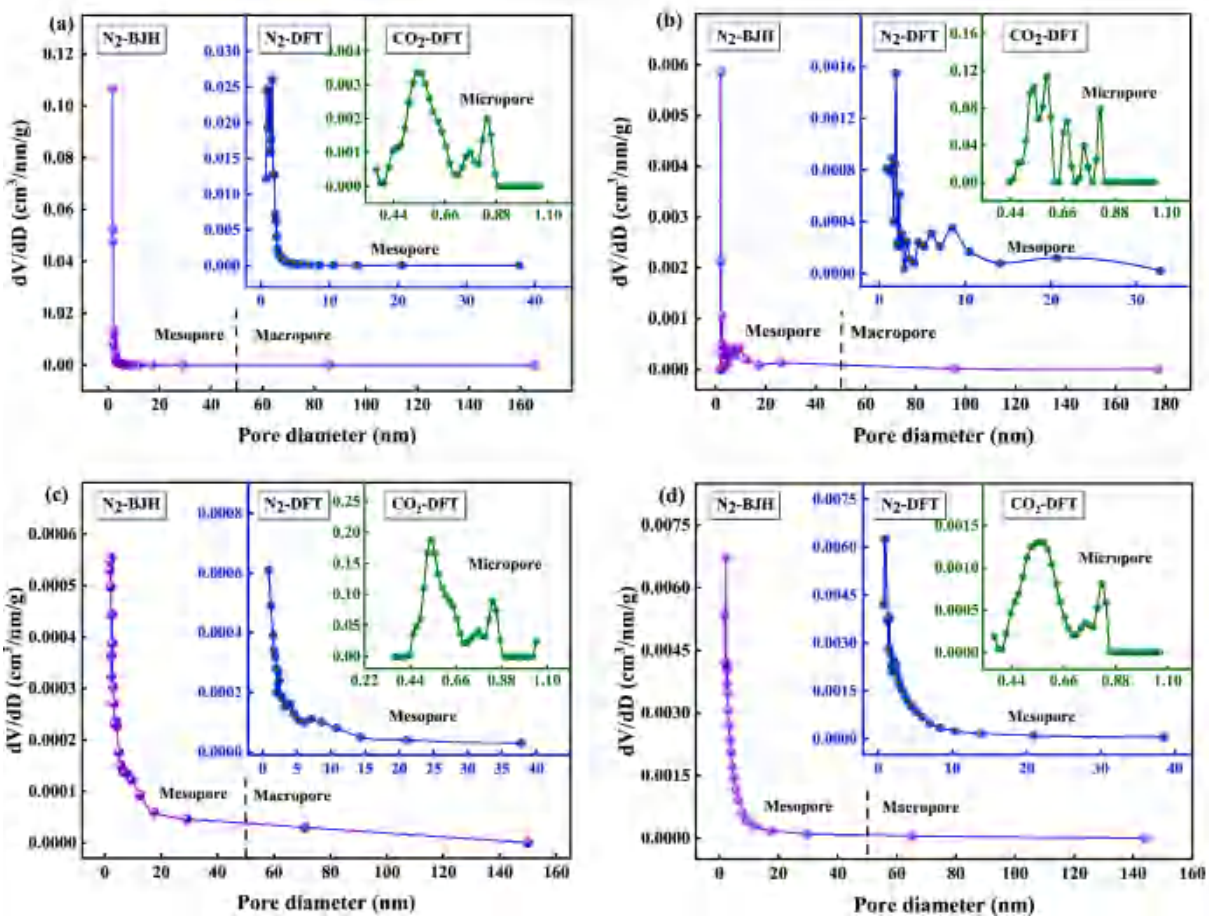

Fig. 6. Pore size distribution of coal based on LPCO$_2$A-LTN$_2$A method:(a) WJB, (b) QL, (c) FR, (d) DLT.

2.1612 nm, respectively; the pore sizes of the developed pores with relatively low coalification degree are larger. The sequence of decreasing overall pore development in the WJB, QL, and FR samples suggests that as the degree of tectonic deformation increases, the size of the developed pores in the coal decreases.

In this study, CO_2-DFT was selected to determine the pore volume (PV) and specific surface area (SSA) of the micropores in coal, as illustrated in Fig. 7a and b. Among the samples, WJB exhibited the highest PV and SSA for its micropores, providing numerous sites for gas surface adsorption. FR coal samples followed, while QL had the lowest values. Additionally, the T-P model (adsorption layer thickness 0.36 nm–1 nm) and the H-K model (1 nm–2 nm) in LTN$_2$A could also ascertain the micropores pore size distribution, along with PV and SSA. These, combined with PV and SSA data from N_2-BJH adsorption, classified pores into micropores (0.36 nm–2 nm), mesopores (2 nm–10 nm and 10 nm–50 nm, note the repetition has been corrected), and macropores (50 nm–200 nm) categories, and plotted their PV and SSA percentages in Fig. 7c and d. Mesopores possessed the largest PV percentage, with a similar trend observed in their SSA. Notably, mesopores ranging from 2 nm–10 nm had a significant SSA percentage, favorable for gas adsorption. WJB contained a comparable percentage of micropores and mesopores (2 nm–10 nm), with relatively few macropores, attributed to the intensity of tectonic deformation. Micropores dominated in samples with a high degree of coaling, and PV contributions from pores 2 nm–10 nm and 10 nm–50 nm were comparable. Furthermore, tectonic deformation increased the number of micro-nano pores below 10 nm. These results are similar to those of previous scholarly studies [51].

3.2. Pore structure characterisation and accessibility analysis of coal

3.2.1. Fractal characterisation of micro and nano pores

Fractal behavior quantifies pore structure complexity in porous media, reflecting adsorbent passage through gases of various diameters and modeling adsorption amounts across scales[52]. The fractal parameters are derived from the fitted adsorption-pressure relationship to quantify pore structure irregularity[53,54]. The fractal curves and fractal dimensions obtained from LPCO$_2$A and LTN$_2$A test data and Eqs. (1) ~ (3) are shown in Fig. 8. The fractal dimension D_m of coal sample micropores follows the order: WJB, FR, DLT, QL. As tectonic damage increases, D_m rises, enhancing micropore complexity and affecting adsorption characteristics. At the same time, the specimen of DLT has a larger D_m, indicating that the development of primary micropores is also the main reason for the change of microporous fractal.

Based on the fractal curves of the LTN$_2$A and FHH models, the fitting within the P/P_0 intervals of 0–0.5 and 0.5–1 yielded D_1 and D_2, which represent the surface roughness of the pores larger than 2 nm and the pore structural features in the coal, respectively. Additionally, the variation range of the composite fractal dimensions D for the P/P_0 interval of 0–1 was obtained, ranging from 2.6587 to 2.8523. The D_1 characterizes the roughness of pore sizes (2 nm–4 nm) obtained at a P/P_0 of 0.5 or less. As tectonic action increases, roughness decreases. Higher metamorphic degrees result in smaller D_1 values for coal samples. Increased tectonic deformation raises D_2 and pore structure complexity. The main reason is that tectonic action increases open pores and connected pores in coal, and long pores and short pores coexist. Increased metamorphism and tectonic intensity correlate with more complex micropores (<2 nm) coal structures and higher gas adsorption potential. Meanwhile, under the influence of tectonic action, the roughness of

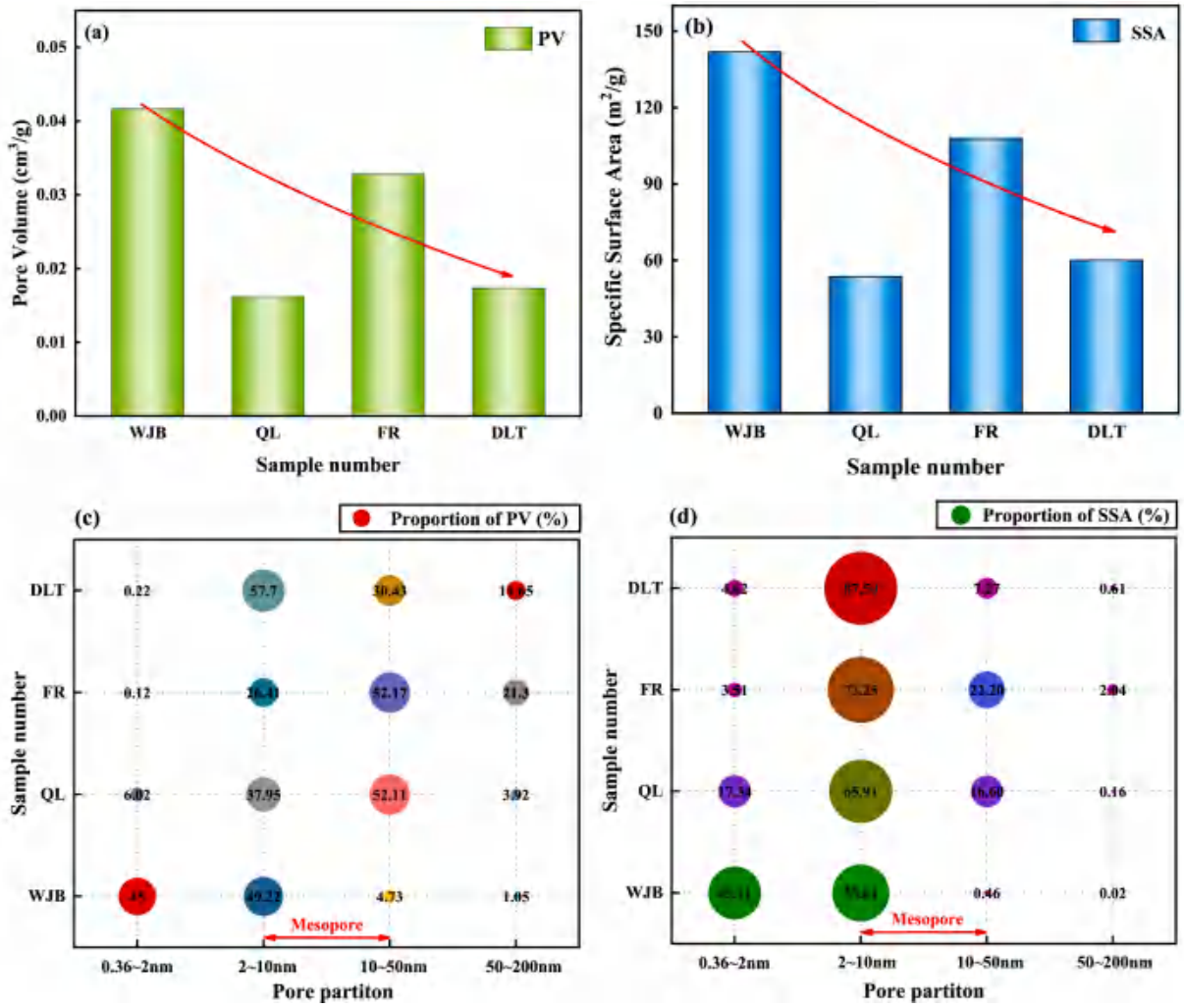

Fig. 7. Stage PV and SSA distributions: (a)~(b) are the micropores PV and SSA obtained for $LPCO_2A$, (c)~(d) are the stage PV and SSA percentage distributions of LTN_2A.

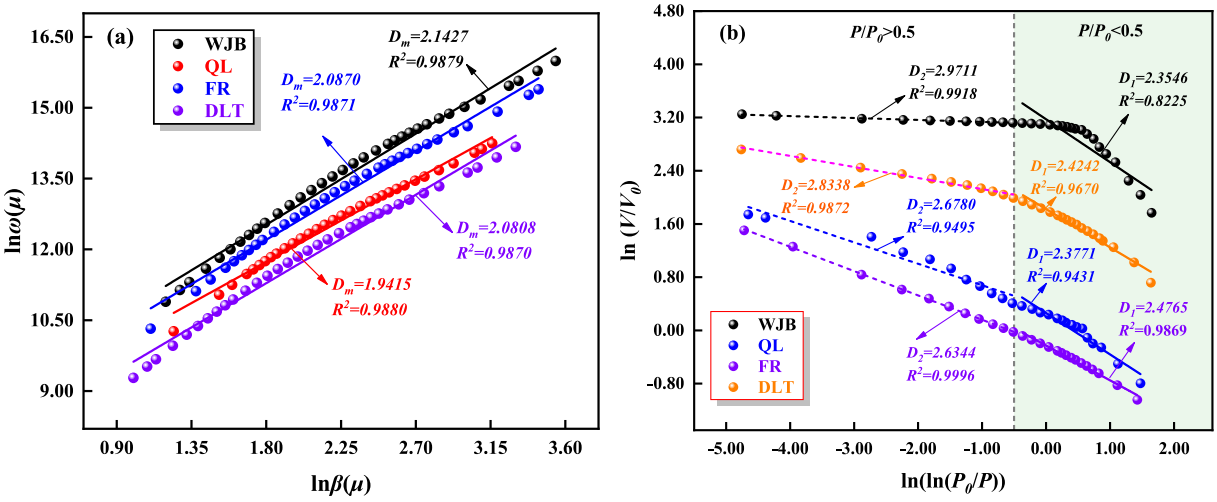

Fig. 8. Micro-nano pore fractal curve of coal: (a) is the fractal dimension of micropores calculated based on $LPCO_2A$, (b) is the fractal dimension of high pressure and low pressure calculated based on LTN_2A.

pores of 2 nm–4 nm decreases, while the pore structure network of pores larger than 4 nm becomes complex.

3.2.2. *Analysis of average pore-throat ratio and pore anisotropy*

P_t represents the comparison between the diameter of the pore cavity and the diameter of the throat. This ratio serves as an indicator of

Table 2
P_t and $A_{ave,total}$ of coal.

Sample number	D_{ave} (nm)	P_t	L_{total}(nm/g)	$lg(A_{ave,total})$ (g^{-1})
WJB	2.2429	60.8674	9.34×10^{18}	16.8354
QL	7.1996	24.7074	2.19×10^{17}	16.4826
FR	10.4455	12.2632	7.82×10^{16}	15.8744
DLT	5.0448	20.3405	1.13×10^{18}	16.0424

Table 3
Pore accessibility (χ) evaluation coefficient of coal.

Sample number	G_1	G_2	χ
WJB	0.1411	8.8712	69.6978
QL	0.1128	0.0138	13.3176
FR	0.1546	0.0019	9.6639
DLT	0.1029	5.4761	90.2635

variations in pore and throat sizes and constitutes a key factor in describing pore structure. A lower P_t signifies a narrower disparity between the diameters of the pore and the throat, facilitating the transport of CBM. On the contrary, the resistance to CBM transport increases. The greater the $A_{ave,total}$, the greater the gas transport resistance. According to the data of LPCO$_2$A and LTN$_2$A and Eqs. (4)~(8), the P_t and $A_{ave,total}$ of coal are shown in Table 2, and the anisotropy $A_{ave,total}$ calculated in the table is relatively large, which is expressed by $lg(A_{ave,total})$.

Comparative analysis of the P_t and $A_{ave,total}$ values of DLT, FR, QL and WJB samples found that the anomalous values of DLT samples are mainly caused by the development of primary micro- nano pore fractures of its coal samples, and its higher pore-throat ratio and anisotropy affect the diffusion efficiency of the gases to a certain degree. The D_{ave} decreases significantly with the increase of the intensity of tectonics, which proves once again that tectonics makes the large pore spaces develop to The D_{ave} decreases significantly with the increase of tectonic intensity, which proves again that the tectonic action makes the large pores develop to the microporous pores. The tectonic action makes the variability of the pore and throat diameters increase, and the P_t shows a significant increase, and the L_{total} per unit of mass coal and the $A_{ave,total}$ increase with the increase of tectonic destructive deformation, and the resistance to the transport of CBM increases. This is also an important reason why it is difficult to desorb, transport and mine CBM in tectonic coal beds.

3.2.3. Pore accessibility analysis

The accessibility(χ) of coal exhibits a strong correlation with the efficacy of gas adsorption and transport processes within micro-nano pore space. Using Eqs. (9) and (10), the pore size distribution curves of CO_2 and N_2 adsorption (Fig. 5) were integrated using the Origin integration function. Form this intergration, solutions were obtained to obtained to determine G_1 and G_2. The evaluation coefficients χ for the specimens were then calculated according to Eq. (11), and the results see

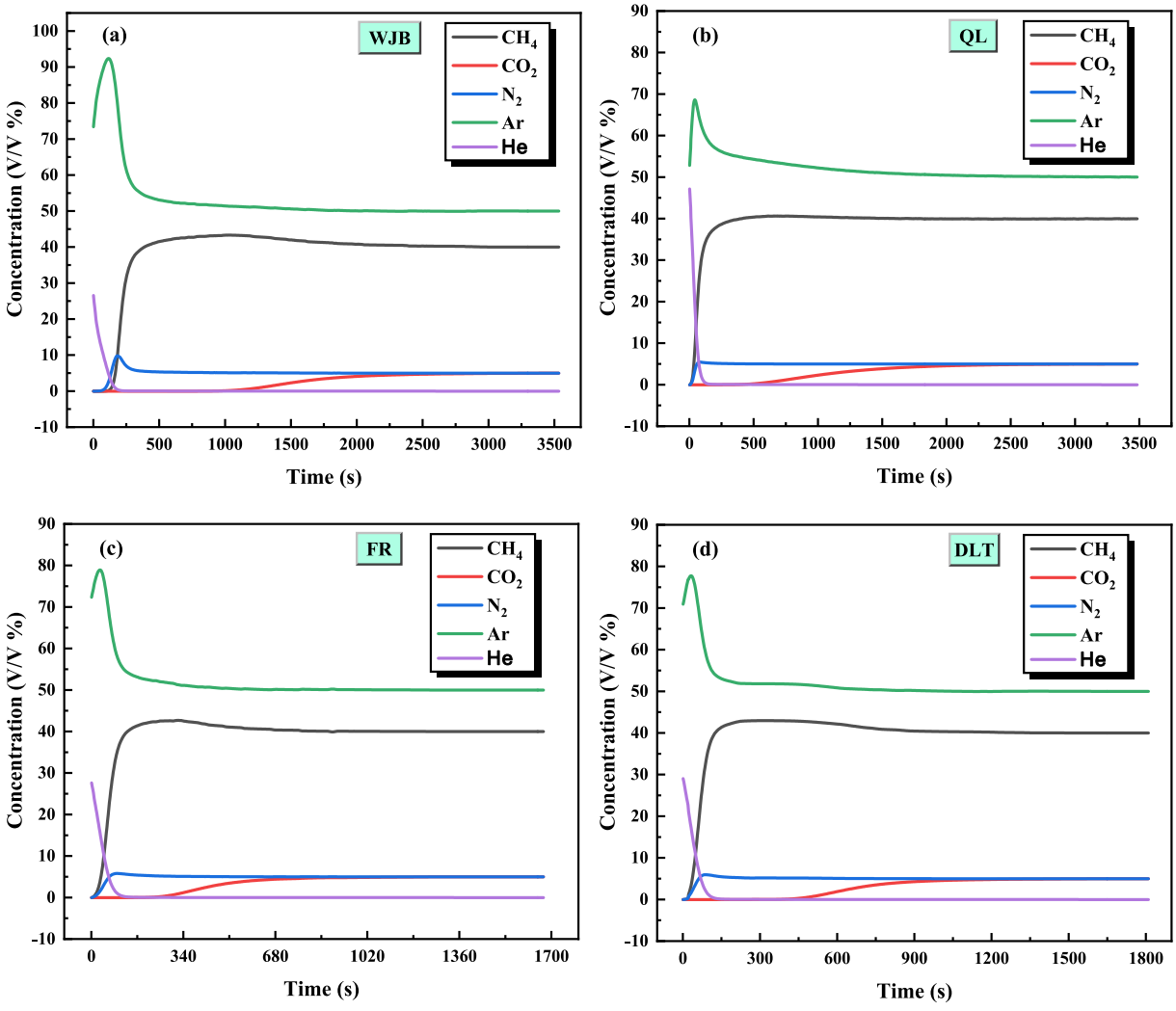

Fig. 9. The concentration curve of each component with time: (a) WJB, (b) QL, (c) FR, and (d) DLT.

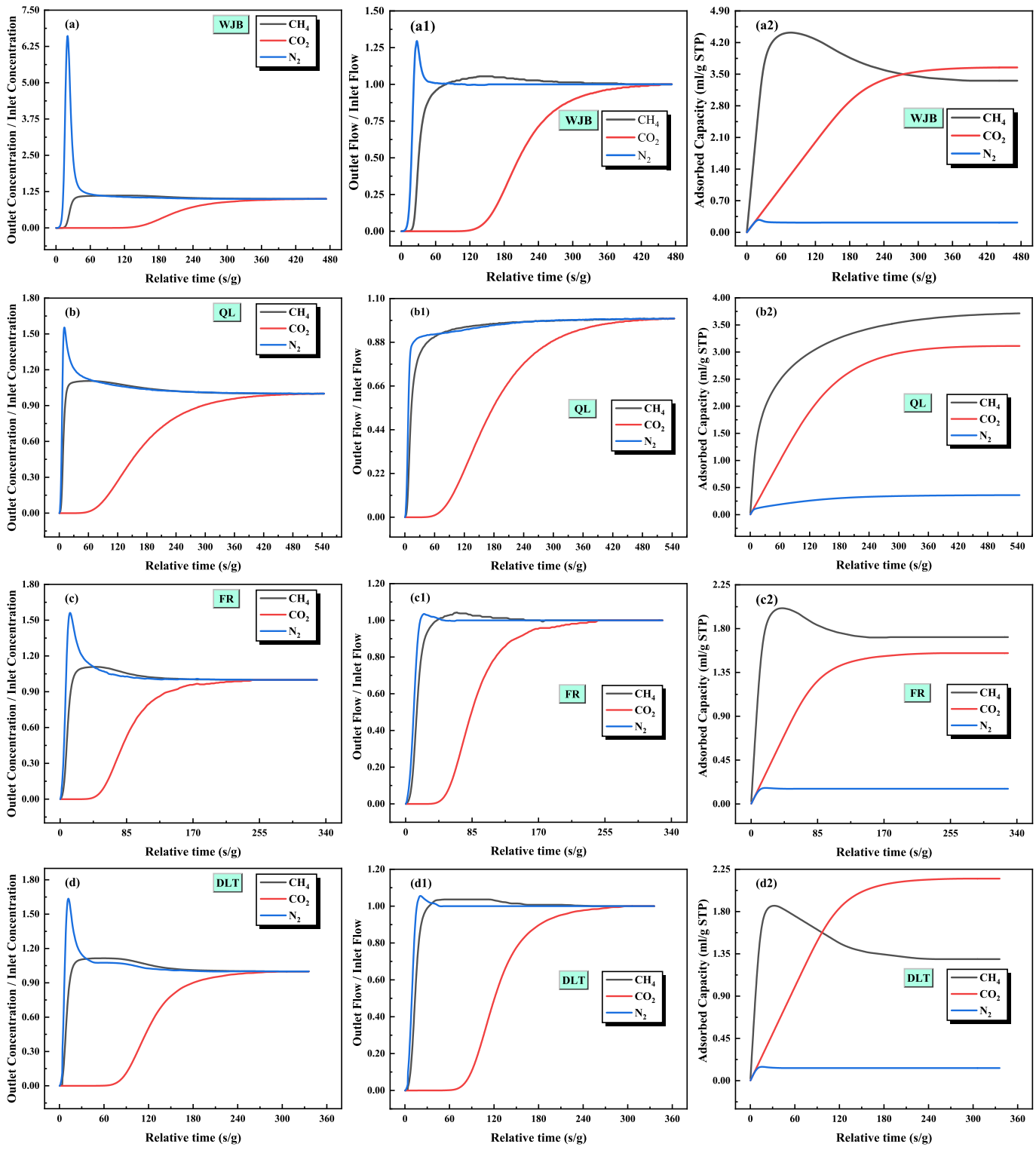

Fig. 10. Multi-component gas adsorption- penetration experimental results: a–d is the penetration curve of outlet concentration/inlet concentration, a1–d1 is the penetration curve of outlet flow/inlet flow, a2–d2 is the penetration curve of adsorption capacity.

Table 3. The χ evaluation coefficients of the specimens were sized as DLT, WJB, QL and FR, which indicates that the pore channel connectivity of DLT samples is strong, and the gas molecules inside the coal body have a fast transport speed, which is conducive to improving the transport efficiency, and the χ of the coal increases with the increase in the intensity of tectonics, which indicates that tectonics promotes pore connectivity to a certain degree of the coal. The χ coefficients of FR samples are diminished, reflecting lower accessibility within micro-nano pore spaces. DLT, a low-rank coal, exhibits significant looseness, larger pores, and an elevated pore accessibility coefficient.

Through a comprehensive evaluation of P_t, $A_{ave,total}$, and χ in coal, it is evident that high P_t and significant $A_{ave,total}$ within the coal's micro-nano pore structure impede gas transport. Furthermore, an elevated χ coefficient indicates enhanced gas adsorption, yet the presence of ink

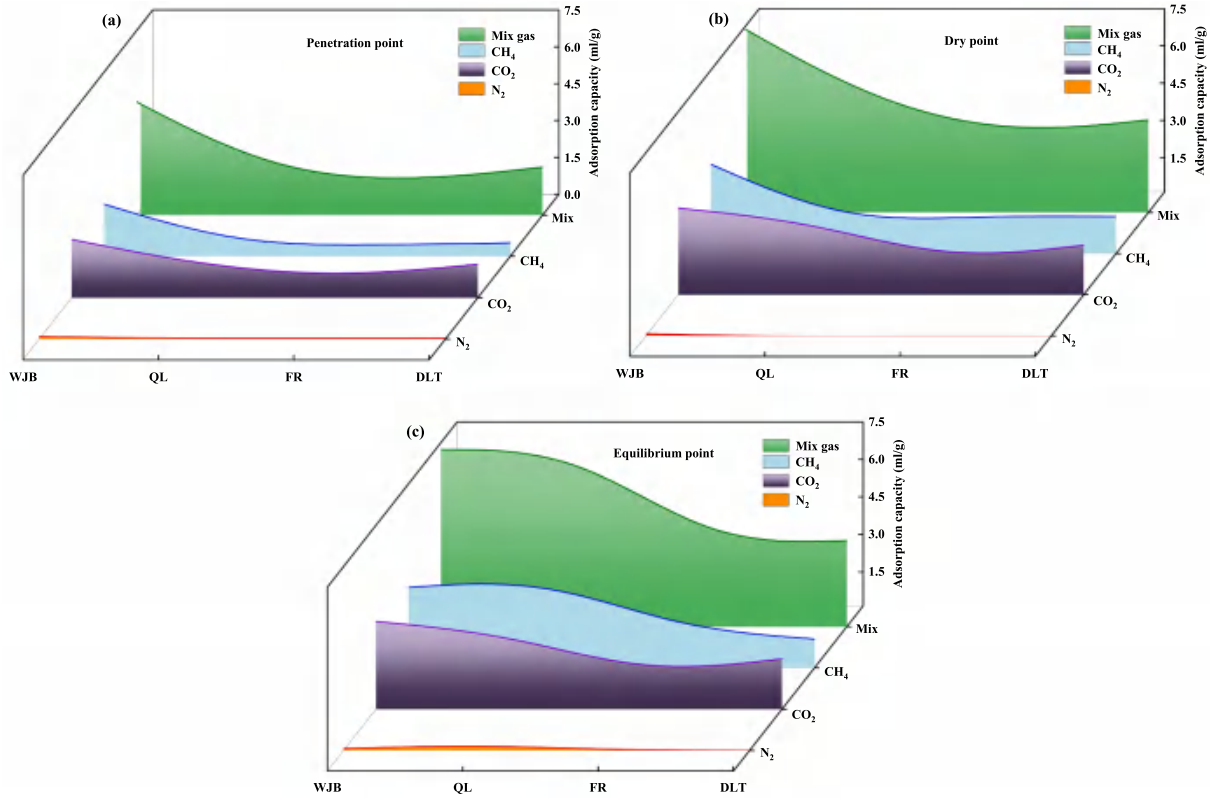

Fig. 11. Adsorption capacity of multi-component gases at (a) penetration point, (b) dry point and (c) equilibrium point.

bottle pores and other non-permissive pore spaces further obstructs gas flow. The WJB and QL samples are subjected to stronger tectonic deformation, and the coals have a large *Pt*, a large anisotropy, complex pore-cracking structure, and there are "ink bottle" pores, and it is more difficult to transport CBM. The average pore throat ratio of DLT and FR samples is small, and the anisotropy values are small, which is conducive to the transport of CBM, among which the χ coefficient of DLT is the largest, and it is assumed that the diffusion efficiency is higher than that of WJB and QL samples. DLT has the largest χ coefficient, so it is assumed that the diffusion efficiency is higher, which will be investigated by multi-component competitive adsorption-penetration test.

3.3. Analysis of competitive adsorption-penetration results for multi-component gases in coal

Competitive adsorption studies of multicomponent gases in coal were mainly realised by molecular simulation in the past [7,55–57], or single-component adsorption tests, and mixed-component gas competitive adsorption tests [33,58,59]. In this study, we explore a novel aspect of CBM adsorption-transport research by examining the competitive adsorption-penetration of mixed gases (CH_4, CO_2, and N_2) using a multicomponent gas competitive adsorption-penetration apparatus, in conjunction with the morphological characteristics of micro- nano pores structures.

The relationship between the concentration of each component gas with time is shown in Fig. 9, when the $CH_4/CO_2/N_2$ gas mixture began to inject, the He concentration from high to the bottom until 0. The reference gas Ar in the mixture of gas injection concentration firstly appeared to rise sharply, and then reached the peak concentration and then began to decline rapidly, and finally the concentration tends to the equilibrium. The concentration of $CH_4/CO_2/N_2$ gas, on the other hand, starts to rise and then tends to the set proportional concentration. N_2 reached the set concentration ratio first in the CO_2/N_2 competition adsorption in coal. In the CH_4/N_2 competition adsorption, although the concentration ratio of CH_4 was much higher than that of N_2, the concentration ratio of N_2 reached the set ratio first, and in CH_4/CO_2 competition adsorption, the concentration ratio of CH_4 reached the set ratio first. It was found that in the $CH_4/CO_2/N_2$ competitive adsorption penetration experiments, the volume concentration values of each component reached equilibrium first in the order of $N_2 > CH_4 > CO_2$ (Langmuir adsorption volume size of $N_2 < CH_4 < CO_2$[60]), which provided a theoretical reference for the set gas ratio of N_2/CO_2 to replace CH_4.

In the multicomponent competitive adsorption-penetration experiments of coal, the penetration curves of each component are an important basis for studying the competitive adsorption characteristics. The gas volume percentage concentration and flow rate penetration curves at the outlet and the inlet, and the adsorption penetration curves are shown in Fig. 10. The order of time taken for the three gases to stabilise is $CO_2 > CH_4 > N_2$. At the initial stage of penetration, the concentration curves of N_2 gas at both the inlet and outlet of the penetration column exhibit the most significant variation (Fig. 10 a–d), attributed to the small adsorption volume of N_2 in coal, which facilitates a rapid attainment of the adsorption volume equilibrium point. CO_2 possesses a substantial adsorption capacity, resulting in a prolonged duration to achieve adsorption equilibrium in the context of competitive adsorption penetration curves. Alternatively stated, the large adsorption volume of CO_2 necessitates an extended period to reach equilibrium within the competitive adsorption penetration framework. Especially in the coal with strong tectonic deformation, it takes longer time to reach the adsorption equilibrium for multi-component gases. The extended adsorption duration observed in DLT coal samples is attributed to the increased pore volume of micropores, offering greater surface area for gas adsorption.

At the penetration point, dry point, and equilibrium point of the multicomponent competitive adsorption-penetration curve, the relative durations for the three gases were sequenced as follows: CO_2 exhibited the longest duration, followed by CH_4, and then N_2. The adsorption

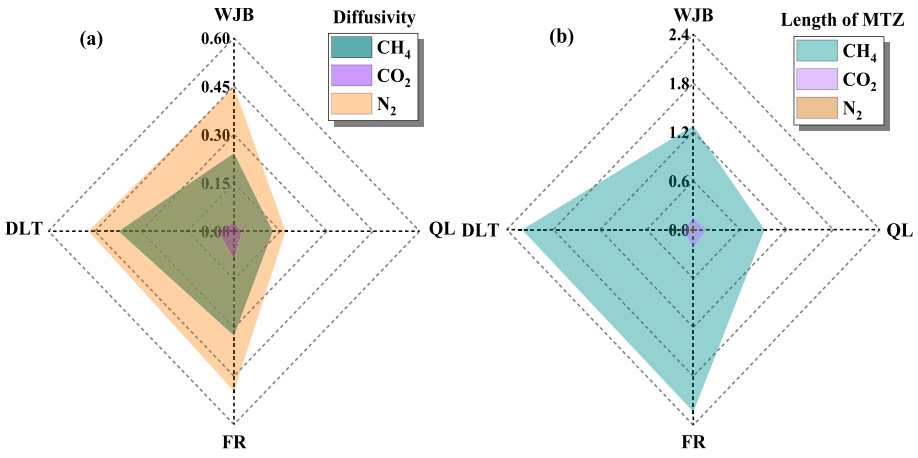

Fig. 12. Diffusion coefficient and mass transfer zone length radar chart.

capacity of CO_2, CH_4, and N_2 in coal followed the order CO_2, CH_4, and N_2. At the penetration and dry points, gas adsorption quantities differed, with a more pronounced distinction under tectonic influence, primarily due to gas adsorption capacity and coal's micro-nanopore structure. Coal micro-nano pore structure, in which the coal pore structure is the degree of micro-nano pore development (micro-nano pore size and number, etc.) affects the adsorption of gas molecules. It was also found that gas adsorption was higher in high order coals than in medium order coals. Furthermore, despite unequal volume percent concentrations of $CH_4/CO_2/N_2$ injected into the penetration column, CO_2 exhibited significantly higher adsorption amounts than the other gases (Fig. 11). This suggests promising applications for CO_2 in enhancing CBM production by displacing CH_4, particularly in high-rank tectonic coals with notable adsorption competition (cf. WJB, QL, and FR samples).

The diffusion coefficients and lengths of mass transfer zones (MTZ) of multicomponent gases in coal reflect their molecular dynamics during competitive adsorption. The sequence of diffusion coefficients for CH_4, CO_2, and N_2 is $N_2 > CH_4 > CO_2$ (Fig. 12). Comparative analysis reveals that CH_4 diffusion coefficients follow the order DLT > FR > WJB > QL, while CO_2 and N_2 coefficients follow FR > DLT > WJB > QL. CH_4, with a larger molecular diameter, cannot diffuse in nanopores < 0.38 nm, explaining its unique diffusion coefficient order. Low-metamorphic coals exhibit higher diffusion coefficients than high-metamorphic coals. Strong tectonic deformation increases "ink bottle" and short pores, enhancing gas adsorption, increasing pore complexity, and reducing diffusion channel efficiency. The MTZ sequence for the gases is

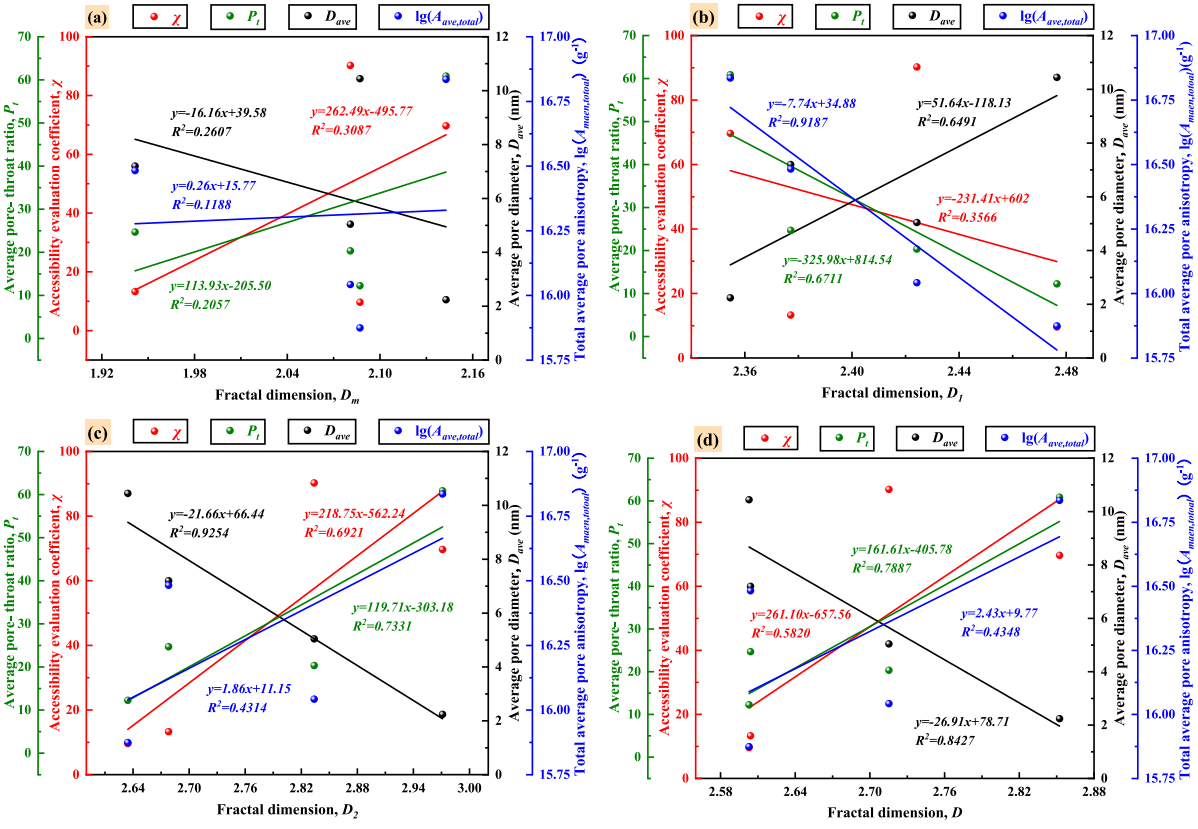

Fig. 13. Relationship between pore structure parameters and fractal dimension: (a) ~ (d) are fitting law of pore χ, average pore throat ratio, average pore diameter and anisotropy with D_m, D_1, D_2, D.

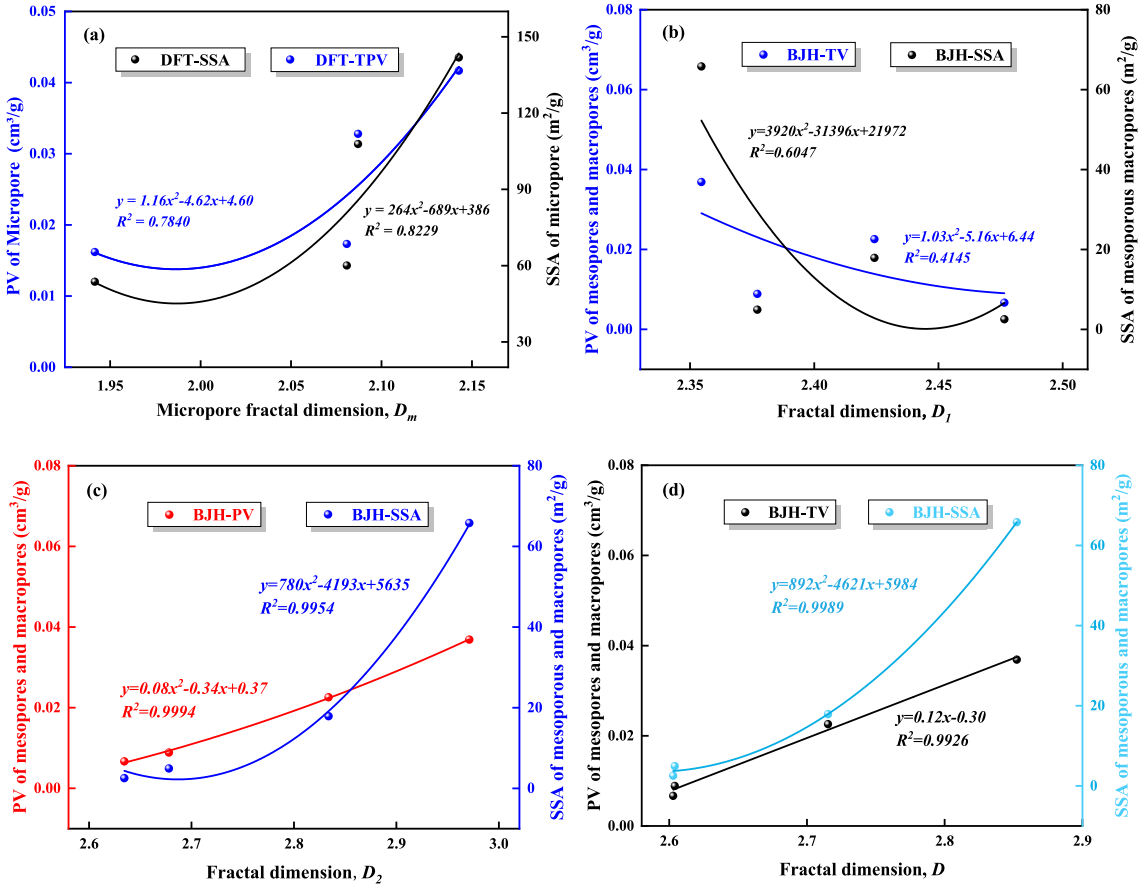

Fig. 14. Relationship between fractal dimension and PV, SSA and adsorption capacity: (a) PV and SSA of micropores and D_m, (b)~(c) PV and SSA of pores larger than 2 nm and D_1, D_2 and D.

$CH_4 > CO_2 > N_2$, with CH_4 and N_2 MTZ lengths ordered FR > DLT > WJB > QL, and CO_2 MTZ lengths FR > QL > WJB > DLT. CBM escape primarily occurs via diffusion; more complex pore-fracture structures prolong the diffusion path, increase resistance, and extend termination time, favoring CBM storage. Similarly, thicker coal seams extend the diffusion path to the roof and floor, increasing diffusion time and favoring storage.

4. Discussions

The micro-nanopore structure in coal determines the competitive adsorption and transport capacity of gases. In this study, we analyzed the effect of pore parameters such as fractal dimension, average pore throat ratio, pore accessibility, and anisotropy on the adsorption and diffusion of multi-component gases from coal. Additionally, we discuss the competitive adsorption and penetration of CH_4, CO_2, and N_2 in micro-nano channels, combining this with multicomponent gas competitive adsorption-penetration experiments that reveal the behaviors of these gases in competitive adsorption and diffusion.

4.1. Effect of micro- nano pore morphology on the adsorption of multi-component gases in coal

The microstructural and morphological attributes of pores within coal at micro- and nanoscale dictate its gas adsorption-diffusion capabilities[61,62]. This study quantitatively investigates the correlation between pore characteristic parameters (D_{ave}, P_t, $A_{ave,\ total}$, and χ), pore fractal dimension, and multi-component gas adsorption-diffusion, subsequently elucidating the gas transport mechanisms within coal's micro-nano pores.

The morphological structure of pores has a close relationship with the fractal dimension of coal pores (see Fig. 13). χ, P_t and $A_{ave,total}$ are positively correlated with the fractal dimensions of micropores D_m, D_2 and D, and the average pore diameter is negatively correlated with D_m, D_2 and D. The average pore diameter is negatively correlated with D_1, and the D_{ave} is positively correlated with D_1. χ, P_t and $A_{ave,total}$ were negatively correlated with fractal dimension D_1 and D_{ave} was positively correlated with D_1. In addition, from the relationship between pore parameters and fractal dimension, χ, P_t and $A_{ave,total}$ correlate well with fractal dimensions D_1, D_2 and D for pores larger than 2 nm. The pore structure parameters (P_t, D_{ave}, A, χ) correlate less well with the fractal dimension of micropores (<2 nm), and additional samples are needed to elucidate their relationship.

The relationships between the microporous specific surface area (SSA), pore volume (PV) and fractal dimensions D_m, D_1, D_2 and the integrated fractal dimension D are shown in Fig. 14. When the fractal dimension was greater than 2, the micropores PV and SSA showed a positive correlation trend with the micropores fractal dimension D_m, i.e., the SSA and Dm increased with the increase of D_m, which indicated that the more complex the micropores were, the stronger the carbon dioxide adsorption capacity was in the three-dimensional space. On the contrary, PV, SSA and D_1 were negatively correlated, which indicated that the greater the pore roughness, the less N_2 adsorption in coal. This finding contradicts previous studies by scholars, suggesting that not all pore roughness enhances N_2 gas adsorption, and that an increase in pore diameter should also be considered to lead to a decrease in gas adsorption. In addition, as molecules are adsorbed, the pore smoothness increases, the number of gas adsorption sites decreases, and the gas adsorption capacity decreases. PV, SSA, and pore fractal dimension D_2 show a positive correlation trend, and the pore volume and specific

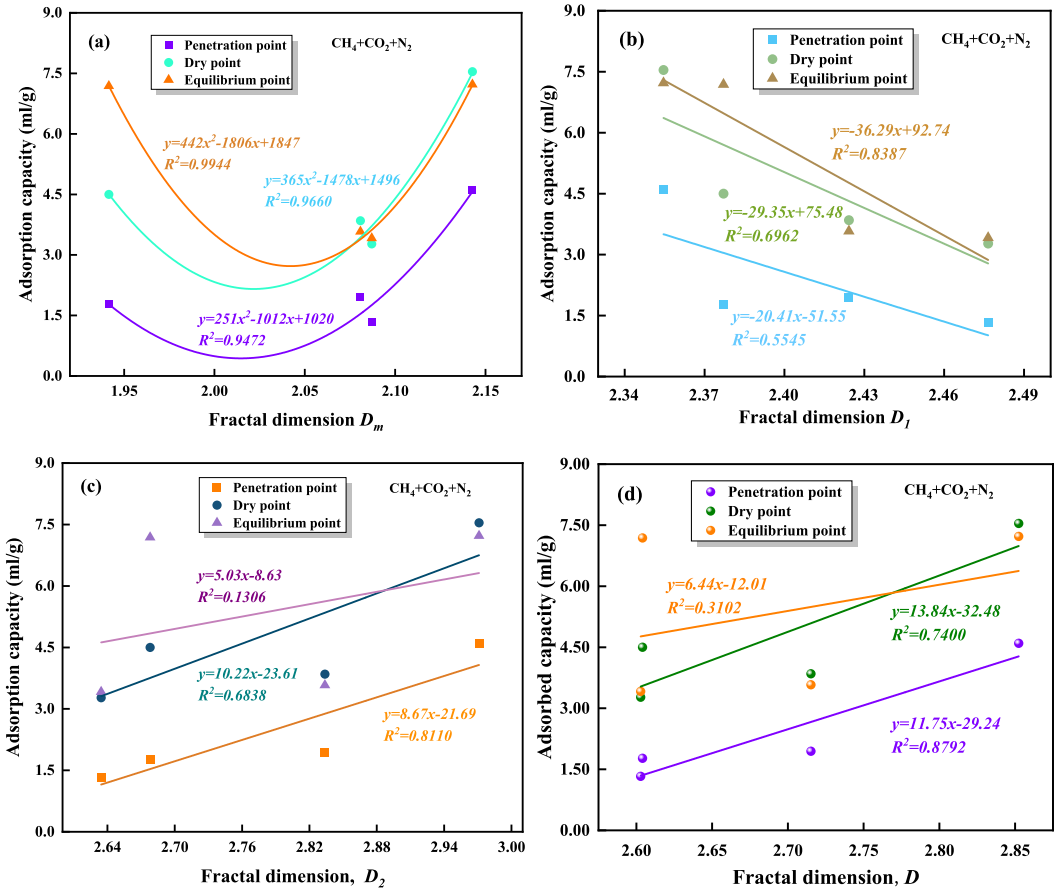

Fig. 15. Relationship between fractal dimension and adsorption capacity of mixed gas: (a) is adsorption capacity and D_m, (b)~(d) are adsorption capacity of pores larger than 2 nm and D_1, D_2 and D.

surface area of the micro- nano pores increase with the increase of the integrated fractal dimension. This indicates that the complexity of micro- and nanopores below 200 nm is directly related to the fractal dimension, and the larger the fractal dimension, the higher the complexity of these pores.

The pore complexity and roughness have an important effect on the competitive adsorption (see Fig. 15). The total adsorption of multi-component gases at the penetration point, drying point and equilibrium point decreases with increasing D_m at D_m less than 2.05, while the total adsorption increases with increasing D_m at D_m greater than 2.05. The fractal dimension between 2 and 3 characterizes the three-dimensional pore space complexity, which indicates that the gas is more easily adsorbed in the larger spatial micropores with more complex pores, while the adsorption decreases with the larger spatial complexity of the micropores in two dimensions. Especially at the penetration point, the competitive adsorption phenomenon was significant, with the adsorption amount of CO_2 being significantly higher than that of CH_4 and N_2. As the fractal dimension of the micropores increased, the total amount of competitive adsorption at the dry point decreased, suggesting that the mode of competitive adsorption during the adsorption process significantly affected the total adsorption amount. The total adsorption amount of multi-component gases at the penetration point, the flow dry point, and the equilibrium point decreased with the increase of D_1. This correlation was stronger than that between the total adsorption amount and the fractal dimension at other pore size stages, indicating that the roughness of the pore surface at the 2 nm–4 nm pore size stage had a greater influence on the total adsorption amount of gases. The decrease in adsorption amount was mainly due to the gases in this nano-pore stage being in the adsorption state and diffusion of the adsorption phase, with CO_2 adsorption reducing pore surface roughness and consequently decreasing CH_4 and N_2 gas adsorption. In contrast, the total adsorption of multi-component gases at the penetration point, the dry point, and the equilibrium point increased with the increase of D_2 and D. This suggested that the more complex the pore structure, the greater the adsorption at the penetration point and the dry point. However, the correlation between the adsorption at the equilibrium point and the fractal dimension was not significant.

The correlation between the adsorption capacity of a multicomponent gas at penetration, dry, and equilibrium points, and the coal metamorphism degree and pore structure characteristics, as shown in Fig. 16. When the average vitrinite reflectivity is greater than 1.8 %, the adsorption capacity exhibits a direct proportionality to vitrinite reflectance, such that an increase in metamorphic degree corresponds to an elevation in gas adsorption capacity in coal. With an increase in coal rank, the adsorption capacities of CO_2, CH_4, and N_2 at the penetration, dry, and equilibrium points increase. The order of gas adsorption capacity among different coal ranks is anthracite > bituminous coal, aligning with Shi et al.[63]. At the penetration point, the adsorption capacity of a single-component gas exhibits the most significant increase with metamorphic degree. In DLT samples, the adsorption capacity of single-component gas is anomalous due to the development of micropores in the coal. However, the overall adsorption capacity of multi-component gases tends to increase. The gas adsorption capacity at the dry point and the equilibrium point also has the same trend. The adsorption capacity of multi-component gas exhibits a strong positive correlation with P_t and $A_{ave,total}$ (Fig. 16c and d). The adsorption capacity increases with the rise in pore χ and $A_{ave,total}$, and this correlation is most pronounced at the penetration point and the dry point. However, the

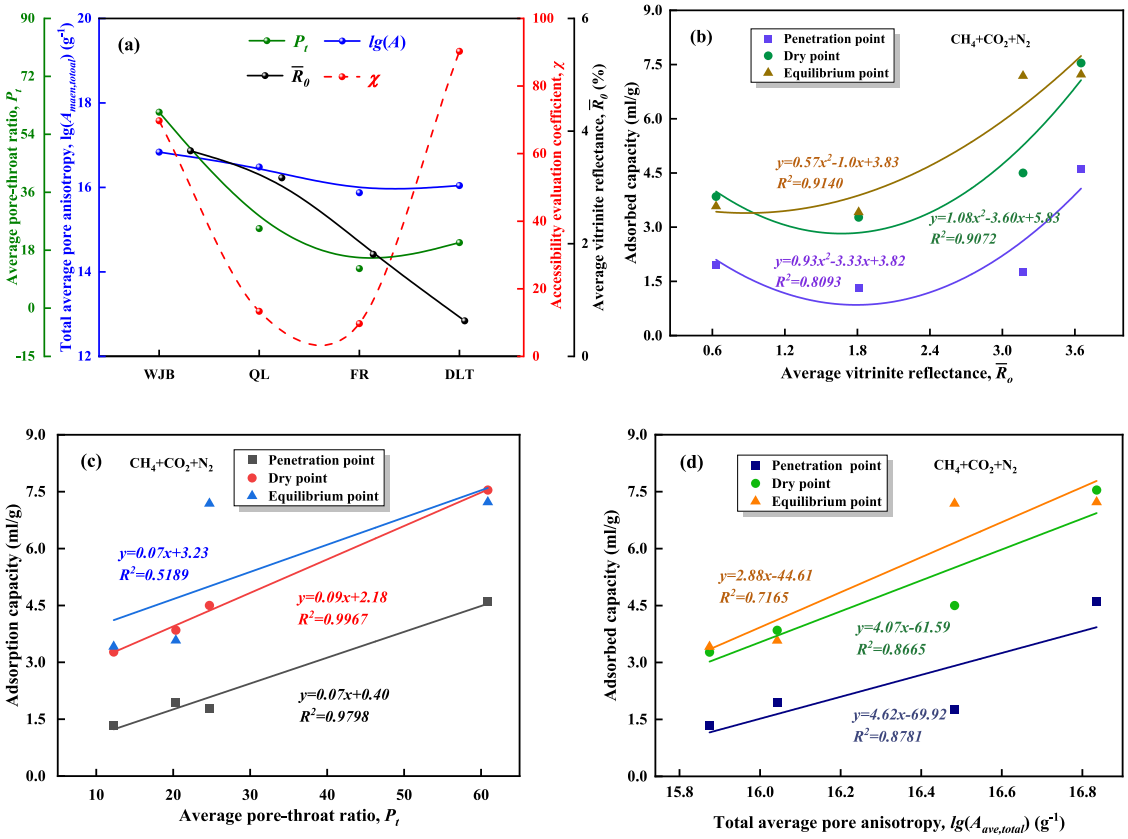

Fig. 16. Relationship between pore structure parameters of coal and multi-component gas: (a) is pore characteristic parameter ($\overline{R}_0$, P_t, A, χ) of different coal samples, (b)~(d) are relationship between the penetration point, dry point and equilibrium point of the mixed gas and the pore characteristic parameter ($\overline{R}_0$, P_t, A).

correlation at the equilibrium point decreases because CO_2/N_2 gases displace part of the CH_4 gas after competitive adsorption. The CH_4 adsorption capacity of QL and FR is higher than that of CO_2 at the dry point and equilibrium point. This is primarily due to the larger average pore size of QL and FR (which provides more adsorption sites) and the injected gas ratio of CH_4: CO_2: N_2 = 8:1:1. The adsorption results of the three gases indicate that CO_2 has a stronger adsorption capacity than CH_4 and N_2. The above research can provide a reference for determining the CO_2/N_2 displacement of CH_4 gas injection ratio and multi-component competitive adsorption time. Additionally, the relationship between total gas adsorption capacity and pore χ is not obvious. However, samples with strong structural deformation exhibit a larger χ, which also results in an increased total gas adsorption capacity (Fig. 11 and Fig. 16a).

4.2. *Effect of micro- nano pore morphology on the diffusion of multi-component gases in coal*

In order to explore the correlation between pore characteristics and diffusion coefficient. The variation trend of diffusion coefficient with P_t, $A_{ave,total}$, χ and fractal dimension as show in Fig. 17. The diffusion coefficient decreases with increasing coal rank because higher coal rank leads to greater density, and matrix pores are generally present. Pores smaller than 2 nm are beneficial for adsorption but unfavorable for gas migration. Similarly, the diffusion coefficient decreases with increasing anisotropy, and a higher $A_{ave,total}$ indicates greater pore heterogeneity and lower gas migration efficiency. The diffusion coefficient increases with the increase in fractal dimensions D_m and D_1, and the reason for the increase of diffusion coefficient is the suction effect of gas in nanoporous channels. At the same time, the study shows that the complexity of the micropore structure has the most significant impact on N_2 diffusion efficiency, followed by CH_4. However, the diffusion efficiency in pores sized 2 nm to 4 nm is also greatly influenced by the pore structure, with CH_4 being affected similarly. As the fractal dimension D increases, the diffusion coefficient of CH_4 and N_2 tends to increase, while the diffusion coefficient of CO_2 decreases, a phenomenon known as reverse diffusion. The correlation between fractal dimension (above 4 nm) and diffusion coefficient is not significant, as gas diffusion in pores is mainly controlled by the pore network and large pore center diffusion, with reduced influence from pore walls. Additionally, FR and DLT coal samples with minor structural deformation exhibit higher diffusion coefficients than WJB and QL samples with significant deformation. This is due to a decrease in medium-long pores and an increase in micro-pores in heavily deformed coal, reducing diffusion efficiency and hindering migration. Among these, FR has the highest diffusion coefficient, attributed to factors like a large average pore diameter, small pore throat ratio, and low anisotropy.

4.3. *Adsorption-penetration mechanism of multi-component gases in micro- nano pore and its implication for CBM extraction*

The optimal gas mixture volume concentration ratio significantly impacts CO_2 geological sequestration and CH_4 recovery enhancement [64]. The gas mixture volume ratio selected in this paper results in a competitive adsorption capacity at the penetration point, with CO_2 > CH_4 > N_2. However, at the flow-drying point and equilibrium point, CH_4 adsorption capacity exceeds CO_2, while N_2 diffusion capacity is greater than both CH_4 and CO_2. The level of coalisation significantly influences gas adsorption [65], with an increase in organic component content in coal samples leading to enhanced adsorption. In competitive adsorption-penetration experiments, gas adsorption and diffusion are affected by micropores and mesopores, respectively, This is consistent with the

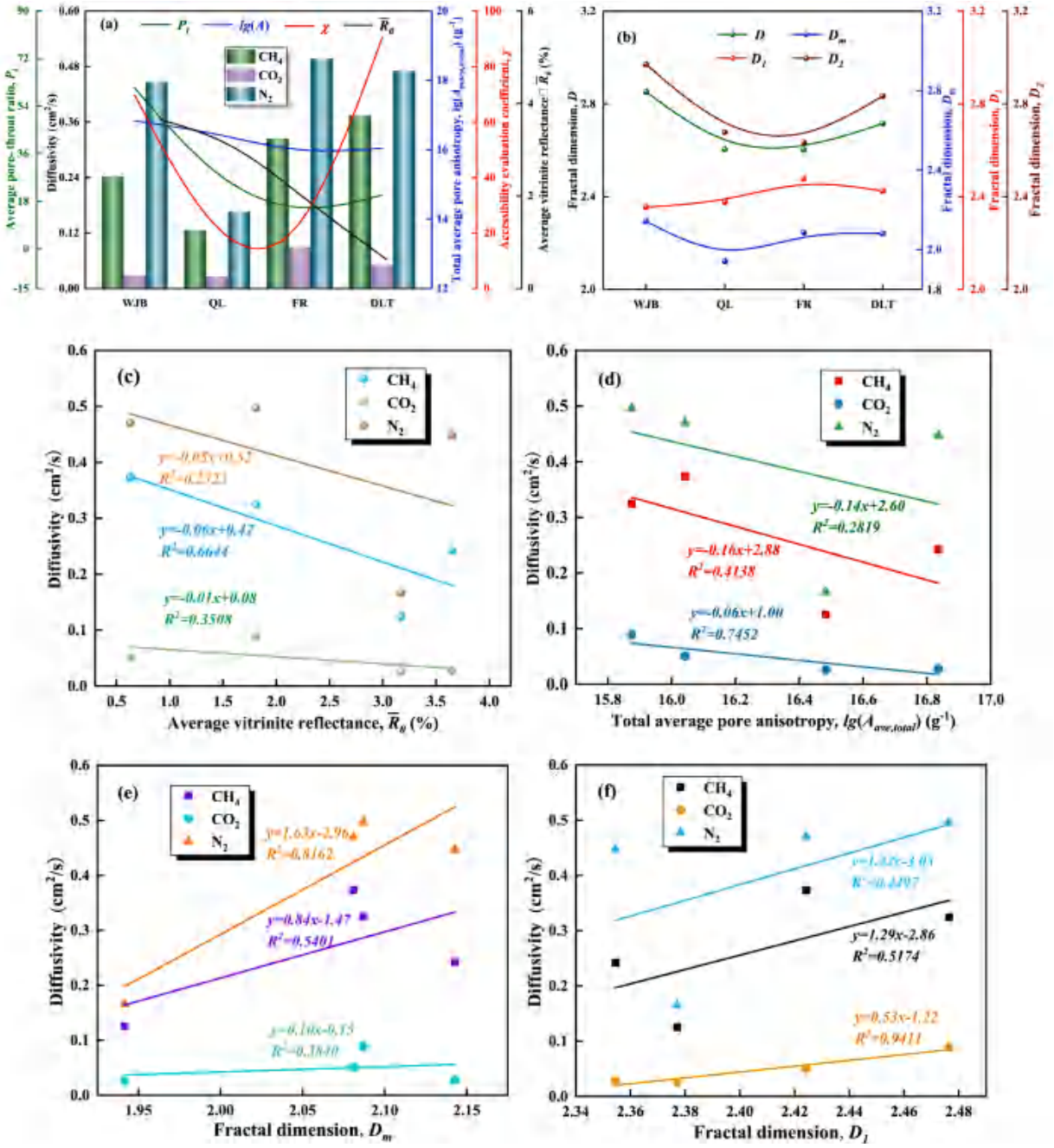

Fig. 17. Difference analysis of diffusion coefficient and pore structure parameters of coal with different degrees of coalification: (a) Difference analysis of diffusion coefficient and pore structure parameters (P_t, D_{ave}, A, χ), (b) Difference between diffusion coefficient and fractal dimension.

results of other scholars who have studied micropores as important pores affecting methane gas adsorption-diffusion [49]. In this paper, the study shows that the fractal dimension increases in 0.36 nm–1.1 nm and the diffusion coefficient of multicomponent gases increases, which indicates that diffusion also exists in micropores smaller than 1.1 nm, mainly by slip. The fractal dimension of pores ranging from 2 to 4 nm is positively correlated with the diffusion of multi-component gases, suggesting that pore complexity within this size range affects diffusion. In the micro-nano pore spaces of coal, the adsorption of multi-phase gases is inversely proportional to their diffusion.

From the schematic diagram of multicomponent competitive adsorption-penetration (Fig. 18), it can be seen that in the competitive adsorption process of CH_4, CO_2 and N_2, among them, N_2 reaches the saturation adsorption point first, but it has little effect on CH_4 adsorption. While CH_4 adsorption decreased during CO_2 gas adsorption, there was gas displacement in this process, and the adsorption phase of CO_2 with high adsorption capacity increased, resulting in a decrease in the adsorption phase of N_2/CH_4. When CO_2 adsorption reaches saturation, then the three gas adsorption reaches equilibrium, and thereafter the diffusion phenomenon. Diffusion in micro- and nanopores is mainly affected by the roughness, pore connectivity, and anisotropy of the coal pore surface.

The limitation of this study is that it does not take into account the study of competitive adsorption of gases with different gas concentration ratios, different temperatures and different pressures. Add experimental tests or molecular simulations with different volume ratios, pressures and temperatures to increase the richness of the study [33,66]. If other volume ratios of multicomponent gases are investigated, such as

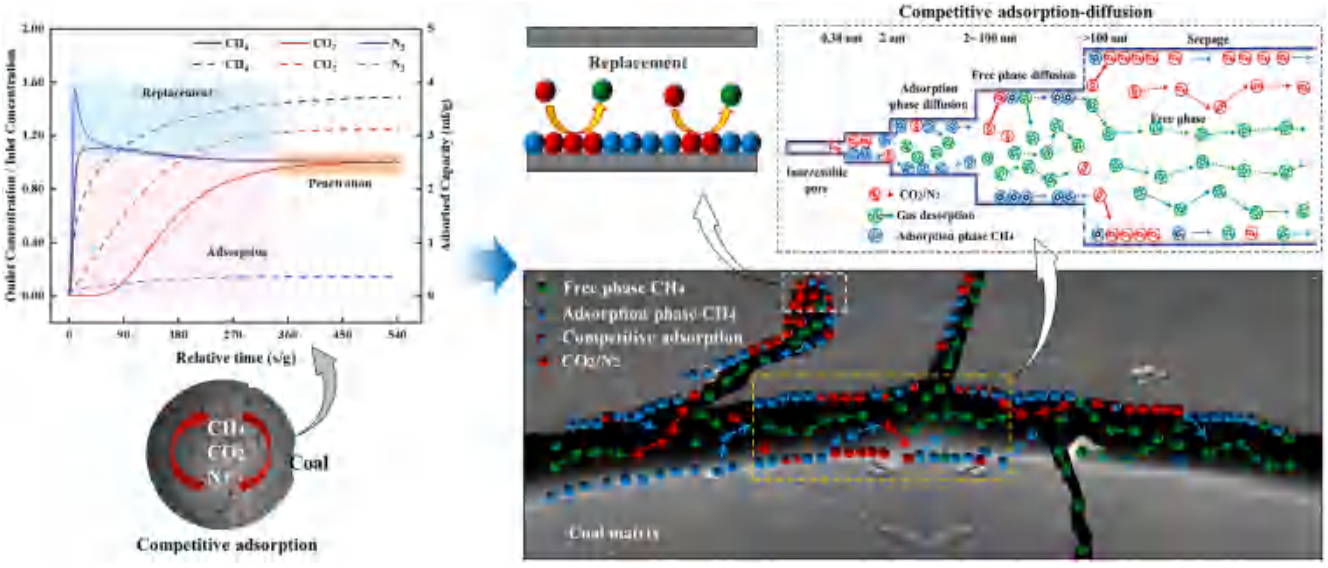

Fig. 18. Competitive adsorption-penetration mechanism diagram of multi-component gas in micro-nano pores.

isovolumetric, and competitive adsorption and permeation at different temperatures, pressures, etc., can be considered, they can provide a reference for determining the optimal ratio, temperature, and pressure for carbon dioxide/nitrogen injection in place of methane.

5. Conclusions

This paper investigates the pore structure characteristics of coal from a microscopic perspective, calculates the pore fractal dimension, P_t, $A_{ave,total}$, χ, and employs the multi-component gas adsorption-penetration experiments to investigate the adsorption-diffusion characteristics of multi-component gases (CH_4, CO_2, and N_2) in coal. The main conclusions are as follows:

(1) The micro-nano pore structure in coal exhibits obvious heterogeneity, and the fractal dimension is evident. The varying morphologies and structures of micropores are the primary reasons for the fractal changes observed in these pores, which provide an excellent environment for gas adsorption. The stronger the tectonic deformation, the greater the difference between pore and throat diameter of coal, resulting in a smaller the D_{ave}, a larger the P_t, a greater the $A_{ave,total}$, and consequently, a greater migration resistance of CBM within the micro-nano pores. In coals with significant structural deformation, the number of "ink bottle" pores and short pores increases notably, which elevates the χ of the micro-nano pores and enhances the adsorption capacity, thereby providing a potential source for diffusion.

(2) χ, P_t, and $A_{ave,total}$ correlate positively with fractal dimensions D_m, D_2, and D, but negatively with D_1. The D_{ave} shows the opposite trend, it correlates negatively with D_m, D_2, and D, and positively with D_1. While the total adsorption increases with increasing Dm at Dm greater than 2.05, as D_m rises, the total adsorption capacity for multi-component gases increases at both the penetration, dry, and equilibrium points. Micropore gas competition significantly impacts total adsorption, with structural coal showing even greater adsorption growth. Conversely, as D_1 increases, total adsorption capacity drops at penetration, dry, and equilibrium points. Here, pore surface roughness plays a crucial role. Post-CO_2 adsorption, roughness decreases, reducing CH_4 and N_2 adsorption. However, as D_2 and D increase, total adsorption capacity for multi-component gases rises at penetration, dry, and equilibrium points.

(3) In a coal-based competitive adsorption-penetration experiment involving CH_4, CO_2, and N_2, the adsorption capacity follows the order: $CO_2 > CH_4 > N_2$. The multicomponent gas adsorption capacity increases with rising χ and $A_{ave,total}$, with the strongest correlation observed at the penetration and dry points. However, at the equilibrium point, the correlation weakens due to CO_2 and N_2 displacing CH_4 after competitive adsorption. The length of the mass transfer zone is ordered as: $CH_4 > CO_2 > N_2$. The diffusion coefficients follow the sequence: $N_2 > CH_4 > CO_2$. During the competitive adsorption-penetration test, suction effect occurs, leading to higher diffusion coefficients in nano-pores smaller than 4 nm. These coefficients increase with fractal dimensions D_m and D_1 but decrease with increasing $A_{ave,total}$. Additionally, higher anisotropy indicates greater pore heterogeneity, resulting in lower gas migration efficiency.

This paper comprehensively evaluates the challenges of micro- and nano-pore structures for gas transport from pore fractal characteristics, P_t, $A_{ave,total}$ and χ evaluation. For CBM extraction, elucidating the adsorption-diffusion mechanism of CH_4, CO_2, and N_2 multi-component gases is of profound significance for the injection of CO_2/N_2-driven CBM to increase the production of CH_4 and the separation of CH_4 from gas mixtures in the process of high-efficiency CBM development.

CRediT authorship contribution statement

Honggao Xie: Writing – original draft, Visualization, Data curation. **Shuxun Sang:** Writing – review & editing, Investigation, Funding acquisition. **Xijian Li:** Writing – review & editing, Supervision, Formal analysis. **Zhihua Yan:** Data curation. **Xiaozhi Zhou:** Methodology, Data curation. **Shiqi Liu:** Methodology, Formal analysis. **Sijie Han:** Methodology, Data curation. **Junjie Cai:** Supervision, Conceptualization.

Declaration of competing interest

The authors declare that they have no known competing financial interests or personal relationships that could have appeared to influence the work reported in this paper.

Acknowledgments

The research was funded by the "Belt and Road" Innovation Cooperation Project of Jiangsu Province (No. BZ2022015), the National Natural Science Foundation of China (No. 42030810), and the National Natural Science Foundation of China Carbon Neutralization Project (No. 42141012).

Data availability

Data will be made available on request.

References

[1] F. Zhou, S. Liu, Y. Pang, J. Li, H. Xin, Effects of coal functional groups on adsorption microheat of coal bed methane, Energy Fuels 29 (2015) 1550–1557, https://doi.org/10.1021/ef502718s.

[2] C. Zhao, Y. Cheng, W. Li, L. Wang, K. Zhang, C. Wang, Critical stress related to coalbed methane migration pattern: model development and experimental validation, Energy 284 (2023) 128681, https://doi.org/10.1016/j.energy.2023.128681.

[3] L. Qin, P. Wang, H. Lin, S. Li, B. Zhou, Y. Bai, D. Yan, C. Ma, Quantitative characterization of the pore volume fractal dimensions for three kinds of liquid nitrogen frozen coal and its enlightenment to coalbed methane exploitation, Energy 263 (2023) 125741, https://doi.org/10.1016/j.energy.2022.125741.

[4] H. Li, C. Xu, G. Ni, J. Lu, Y. Lu, S. Shi, M. Li, Q. Ye, Spectroscopic (ftir, 1h nmr) and sem investigation of physicochemical structure changes of coal subjected to microwave-assisted oxidant stimulation, Fuel 317 (2022) 123473, https://doi.org/10.1016/j.fuel.2022.123473.

[5] Z. Niu, X. Cui, T. Pham, P.C. Lan, H. Xing, K.A. Forrest, L. Wojtas, B. Space, S. Ma, A metal–organic framework based methane nano-trap for the capture of coal-mine methane, Angew. Chem. Int. Ed. 58 (2019) 10138–10141, https://doi.org/10.1002/anie.201904507.

[6] C. Xu, W. Wang, K. Wang, A. Zhou, L. Guo, T. Yang, Filling–adsorption mechanism and diffusive transport characteristics of N_2/CO_2 in coal: experiment and molecular simulation, Energy 282 (2023) 128428, https://doi.org/10.1016/j.energy.2023.128428.

[7] Z. Li, Y. Bai, H. Yu, H. Hu, Y. Wang, Molecular simulation of thermodynamic properties of CH_4 and CO_2 adsorption under different moisture content and pore size conditions, Fuel 344 (2023) 127833, https://doi.org/10.1016/j.fuel.2023.127833.

[8] Z. Wang, S. Sang, X. Zhou, S. Liu, H. Wang, Y. Shu, Response in coal reservoirs and in-situ stress control during horizontal well coal cavern completion and stress release, Gas Sci. Eng. 113 (2023) 204950, https://doi.org/10.1016/j.jgsce.2023.204950.

[9] S. Sang, H. Xu, L. Fang, G. Li, H. Huang, Stress relief coalbed methane drainage by surface vertical wells in china, Int. J. Coal Geol. 82 (2010) 196–203, https://doi.org/10.1016/j.coal.2009.10.016.

[10] H. Xie, X. Li, Microstructure and nanomechanical characterization of tectonic coal based on sem, afm, xrd and dsi, Surf. Interfaces 46 (2024) 104158, https://doi.org/10.1016/j.surfin.2024.104158.

[11] I. Shovkun, D.N. Espinoza, Propagation of toughness-dominated fluid-driven fractures in reactive porous media, Int. J. Rock Mech. Min. Sci. 118 (2019) 42–51, https://doi.org/10.1016/j.ijrmms.2019.03.017.

[12] P. Mou, J. Pan, K. Wang, J. Wei, Y. Yang, X. Wang, Influences of hydraulic fracturing on microfractures of high-rank coal under different in-situ stress conditions, Fuel 287 (2021) 119566, https://doi.org/10.1016/j.fuel.2020.119566.

[13] S. Sang, X. Zhou, S. Liu, H. Wang, L. Cao, H. Liu, Z. Li, S. Zhu, C. Liu, H. Huang, H. Xu, R. Wamg, J. Jia, T. Ashutosh, S. Han, Research advances in theory and technology of the stress release applied extraction of coalbed methane from tectonically deformed coals, J. China Coal Soc. 45 (2020) 2531–2543, https://doi.org/10.13225/j.cnki.jccs.DZ20.0754.

[14] H. Lin, H. Long, S. Li, Y. Bai, T. Xiao, A. Qin, CH_4 adsorption and diffusion characteristics in stress-loaded coal based on molecular simulation, Fuel 333 (2023) 126478, https://doi.org/10.1016/j.fuel.2022.126478.

[15] J. Han, A.K. Bogomolov, E.Y. Makarova, Z. Yang, Y. Lu, X. Li, Molecular simulations on adsorption and diffusion of co2 and ch4in moisture coals, Energy Fuels 31 (2017) 13528–13535, https://doi.org/10.1021/acs.energyfuels.7b02898.

[16] J. Gao, X. Li, Y. Shi, S. Jia, X. Ye, Y. Long, The adsorption model of the adsorption process of ch4 on coal and its thermodynamic characteristics, Colloids Surf. A Physicochem. Eng. Asp. 632 (2022) 127766, https://doi.org/10.1016/j.colsurfa.2021.127766.

[17] Z. Xu, Q. Liu, Q. Zheng, H. Cheng, Y. Wu, Isotopic composition and content of coalbed methane production gases and waters in karstic collapse column area, qinshui coalfield, china, J. Geochem. Explor. 165 (2016) 94–101, https://doi.org/10.1016/j.gexplo.2016.03.001.

[18] B. Zhou, Q. Zhou, K. Yang, H. Xin, M. Ran, J. Hou, Z. Deng, B. Qin, Research on the wetting interface characteristics between water molecules and bituminous coal based on pore evolution and molecular dynamic theory, Energy 297 (2024) 131169, https://doi.org/10.1016/j.energy.2024.131169.

[19] S. Han, S. Wang, C. Guo, S. Sang, A. Xu, W. Gao, P. Zhou, Distribution of the adsorbed density of supercritical CO_2 onto the anthracite and its implication for co2 geologic storage in deep coal, Geoenergy Sci. Eng. 234 (2024) 212624, https://doi.org/10.1016/j.geoen.2023.212624.

[20] X. Ni, J. Miao, R. Lv, X. Lin, Quantitative 3d spatial characterization and flow simulation of coal macropores based on μCT technology, Fuel 200 (2017) 199–207, https://doi.org/10.1016/j.fuel.2017.03.068.

[21] X. Qin, T. Yang, Z. Liu, Q. Liu, Molecular structure, bond cleavage and their relation of four low rank coals, Fuel Process. Technol. 236 (2022) 107391, https://doi.org/10.1016/j.fuproc.2022.107391.

[22] X. Wang, J. Pan, K. Wang, T. Ge, J. Wei, W. Wu, Characterizing the shape, size, and distribution heterogeneity of pore-fractures in high rank coal based on x-ray ct image analysis and mercury intrusion porosimetry, Fuel 282 (2020) 118754, https://doi.org/10.1016/j.fuel.2020.118754.

[23] Y. Li, J. Pan, N. Cheng, Z. Wang, L. Zhang, W. Liu, Relationship between micropore structure of different coal ranks and methane diffusion, Nat. Resour. Res. 31 (2022) 2901–2917, https://doi.org/10.1007/s11053-022-10108-w.

[24] Z. Liu, J. Han, H. Yang, J. Lv, S. Dong, A new model for coal gas seepage based on fracture-pore fractal structure characteristics, Int. J. Rock Mech. Min. Sci. 173 (2024) 105626, https://doi.org/10.1016/j.ijrmms.2023.105626.

[25] H.W. Zhou, L. Zhang, X.Y. Wang, T.L. Rong, L.J. Wang, Effects of matrix-fracture interaction and creep deformation on permeability evolution of deep coal, Int. J. Rock Mech. Min. Sci. 127 (2020) 104236, https://doi.org/10.1016/j.ijrmms.2020.104236.

[26] J. Meng, S. Zhang, Z. Cao, C. Wang, Pore structure characterization based on the panxi coal molecular model, Nat. Resour. Res. 31 (2022) 2731–2747, https://doi.org/10.1007/s11053-022-10085-0.

[27] J. Yang, B. Li, J. Li, H. Song, S. Duan, L. Jia, Theoretical study of shale gas adsorption under the action of moisture and temperature, including analysis of the relevant adsorption mechanisms and thermodynamics, Ind. Eng. Chem. Res. 63 (2024) 617–635, https://doi.org/10.1021/acs.iecr.3c02874.

[28] Y. Ding, B. Li, J. Li, S. Duan, H. Song, X. Zeng, A study of gas transport mechanisms in shale's confined nanopores: examining irregularity, adsorption effects, and stresses, Phys. Fluids 35 (2023) 126108, https://doi.org/10.1063/5.0172862.

[29] Q. Han, C. Deng, T. Gao, Z. Jin, Molecular simulation on competitive adsorption differences of gas with different pore sizes in coal, Molecules 27 (2022) 1594, https://doi.org/10.3390/molecules27051594.

[30] B. Liu, H. Wen, X. Cheng, S. Fan, W. Mi, R. Li, Competitive adsorption law of multi-component gases during co2 displacement of ch4 in coal seams, J. CO_2 Util. 76 (2023) 102581, doi: 10.1016/j.jcou.2023.102581.

[31] Y. Hu, S. Wang, Y. He, Investigation of the coal oxidation effect on competitive adsorption characteristics of co2 /ch4, Energy Fuels 34 (2020) 12860–12869, https://doi.org/10.1021/acs.energyfuels.0c02497.

[32] J. Jia, H. Song, P. Jia, Selective adsorption mechanism of $CO_2/CH_4/N_2$ multi-component gas mixtures by n/s atoms and functional groups in coal, Process Saf. Environ. Protect. 182 (2024) 210–221, https://doi.org/10.1016/j.psep.2023.11.079.

[33] H. Pan, M. Han, T. Zhang, B. Ji, M. Pan, Z. Li, S. Zhu, Influencing factors and adsorption process of N_2 /CH_4 /CO_2 competitive adsorption in coal, Energy Fuels 38 (2024) 22182–22191, https://doi.org/10.1021/acs.energyfuels.4c04363.

[34] B. Zhang, S. Li, Determination of the surface fractal dimension for porous media by mercury porosimetry, Ind. Eng. Chem. Res. 34 (1995) 1383–1386, https://doi.org/10.1021/ie00043a044.

[35] F. Wang, S. Li, Determination of the surface fractal dimension for porous media by capillary condensation, Ind. Eng. Chem. Res. 36 (1997) 1598–1602, https://doi.org/10.1021/ie960555w.

[36] J. Cui, X. Niu, G. Feng, Y. Han, Z. Li, Effect of division methods of the adsorption isotherm on the fractal dimension of clay minerals calculated based on the frenkel–halsey–hill model, Energy Fuels 35 (2021) 8786–8798, https://doi.org/10.1021/acs.energyfuels.1c00876.

[37] W. Chengyang, H. Shixiong, S. Wenjing, C. Wei, Fractal dimension of coal particles and their ch4 adsorption, Int. J. Min. Sci. Technol. 22 (2012) 855–858, https://doi.org/10.1016/j.ijmst.2012.11.003.

[38] P. Pfeifer, M. Obert, M.W. Cole, M. Fleischmann, D.J. Tildesley, R.C. Ball, Fractal bet and fhh theories of adsorption: a comparative study, Proc. R. Soc. London. A 423 (1997) 169–188, https://doi.org/10.1098/rspa.1989.0049.

[39] A. Margellou, P. Pomonis, The total and the differential mean pore anisotropy in porous solids and the ranking of pores according to zipf`s law, Phys. Chem. Chem. Phys. (2017) 1408–1419, https://doi.org/10.1039/C6CP07680G.

[40] M.V. López-Ramón, J.O. Jagie, T.J. Bandosz, N.A. Seaton, Determination of the pore size distribution and network connectivity in microporous solids by adsorption measurements and monte carlo simulation, Langmuir 13 (1997) 4435–4445.

[41] Q. Cai, A. Buts, M.J. Biggs, N.A. Seaton, Evaluation of methods for determining the pore size distribution and pore-network connectivity of porous carbons, Langmuir 23 (2007) 8430–8440, https://doi.org/10.1021/la7007057.

[42] L. Zhang, N.A. Seaton, Simulation of catalyst fouling at the particle and reactor levels, Chem. Eng. Sci. 51 (1996) 3257–3272, https://doi.org/10.1016/0009-2509(95)00388-6.

[43] Q.G. Cen, M.X. Fang, J.P. Xu, Z.Y. Luo, Experimental study of breakthrough adsorption on activated carbon for co2 capture, Adv. Mat. Res. 356–360 (2012) 1139–1144.

[44] S. Fu, B. Tan, G. Cheng, H. Wang, X. Fang, Z. Shao, Z. Li, Study of adsorption characteristics of CO_2, O_2, and N_2 in coal micropores and mesopores at normal pressure, Ind. Eng. Chem. Res. 61 (2022) 12845–12856, https://doi.org/10.1021/acs.iecr.2c01911.

[45] F. Xin, H. Xu, D. Tang, C. Cao, Differences in accumulation patterns of low-rank coalbed methane in china under the control of the first coalification jump, Fuel 324 (2022) 124657, https://doi.org/10.1016/j.fuel.2022.124657.

[46] J. Zheng, X. Liu, Y. Jin, J. Dong, Q. Wang, Effects of surface geometry on advection–diffusion process in rough fractures, Chem. Eng. J. 414 (2021) 128745, https://doi.org/10.1016/j.cej.2021.128745.

[47] Z. Li, T. Ren, X. Li, M. Qiao, X. Yang, L. Tan, B. Nie, Multi-scale pore fractal characteristics of differently ranked coal and its impact on gas adsorption, Int. J. Min. Sci. Technol. 33 (2023) 389–401, https://doi.org/10.1016/j.ijmst.2022.12.006.

[48] Z. Zhang, G. Liu, X. Wang, R. Lv, H. Liu, J. Lin, G. Barakos, P. Chang, A fractal langmuir adsorption equation on coal: principle, methodology and implication, Chem. Eng. J. 488 (2024) 150869, https://doi.org/10.1016/j.cej.2024.150869.
[49] B. Hu, Y. Cheng, Z. Pan, Classification methods of pore structures in coal: a review and new insight, Gas Sci. Eng. 110 (2023) 204876, https://doi.org/10.1016/j.jgsce.2023.204876.
[50] M. Thommes, K. Kaneko, A.V. Neimark, J.P. Olivier, F. Rodriguez-Reinoso, J. Rouquerol, K.S.W. Sing, Physisorption of gases, with special reference to the evaluation of surface area and pore size distribution (iupac technical report), Pure Appl. Chem. 87 (2015) 1051–1069, https://doi.org/10.1515/pac-2014-1117.
[51] S. Yu, J. Bo, L. Ming, H. Chenliang, X. Shaochun, A review on pore-fractures in tectonically deformed coals, Fuel 278 (2020) 118248, https://doi.org/10.1016/j.fuel.2020.118248.
[52] X. Zhang, Fractal character of coal nanopore and effect of deviation corrected, coal rank, and gas adsorption, Microporous Mesoporous Mat. 367 (2024) 112972, https://doi.org/10.1016/j.micromeso.2023.112972.
[53] K. Zhang, J. Li, L. Wang, S. Fu, H. Zhang, X. Xing, Scale-span feature of surface analysis, macromolecular and pore structure in coal: implications for inherent evolutionary mechanism of morphological microstructure, Powder Technol. 448 (2024) 120338, https://doi.org/10.1016/j.powtec.2024.120338.
[54] Y. Yao, D. Liu, D. Tang, S. Tang, W. Huang, Fractal characterization of adsorption-pores of coals from north china: an investigation on ch4 adsorption capacity of coals, Int. J. Coal Geol. 73 (2008) 27–42, https://doi.org/10.1016/j.coal.2007.07.003.
[55] H. Long, H. Lin, M. Yan, P. Chang, S.G. Li, Y. Bai, Molecular simulation of the competitive adsorption characteristics of CH_4, CO_2, N_2, and multicomponent gases in coal, Powder Technol. 385 (2021) 348–356, https://doi.org/10.1016/j.powtec.2021.03.007.
[56] J. Jia, Y. Xing, B. Li, P. Jia, Y. Wu, Q. Yang, D. Wang, Molecular simulations of multivariate competitive adsorption of CH_4, CO_2 and H_2O in gas-fat coal, Colloids Surf. A Physicochem. Eng. Asp. 683 (2024) 132917, https://doi.org/10.1016/j.colsurfa.2023.132917.
[57] Y. Li, Z. Yang, X. Ju, A. Zhou, Adsorption and diffusion behavior of CH_4 and CO_2 in closed and open pores from zhaozhuang coal, Energy Fuels 36 (2022) 2582–2590, https://doi.org/10.1021/acs.energyfuels.1c04262.
[58] H. Yang, N. Kang, X. Chen, Y. Liu, Exploring the inhibitory effect of H_2O on CO_2/CH_4 adsorption in coal: insights from experimental and simulation approaches, Energy 284 (2023) 129317, https://doi.org/10.1016/j.energy.2023.129317.
[59] R. Ma, Y. Yao, M. Wang, X. Dai, A. Li, CH_4 and CO_2 adsorption characteristics of low-rank coals containing water: an experimental and comparative study, Nat. Resour. Res. 31 (2022) 993–1009, https://doi.org/10.1007/s11053-022-10026-x.
[60] Y. Cui, Q. Zhang, H. Zhang, Adsorption of different rank coals to single component gases, Nat. Gas Ind. 25 (2005) 61–68.
[61] L. Wang, G. Zhang, J. Liu, X. Chen, Z. Li, Effect of the pore structure on adsorption and diffusion migration of different rank coal samples, Energy Fuels 34 (2020) 12486–12504, https://doi.org/10.1021/acs.energyfuels.0c02587.
[62] Z. Shao, B. Tan, Y. Guo, T. Li, X. Li, X. Fang, F. Wang, Q. Zhang, H. Wang, Visualization and analysis of mapping knowledge domains for coal pores studies, Fuel 320 (2022) 123761, https://doi.org/10.1016/j.fuel.2022.123761.
[63] Y. Shi, X.A. Yang, J.H. Xue, P.X. Zhao, J.K. Liu, Z.Y. Wei, Investigation of competitive adsorption and diffusion behaviors of co2/ch4/n2/h2o affected by coal ranks in slit structures, J. Porous Media 26 (2023) 15–30.
[64] Z. Fan, G. Fan, D. Zhang, L. Zhang, S. Zhang, S. Liang, W. Yu, Optimal injection timing and gas mixture proportion for enhancing coalbed methane recovery, Energy 222 (2021) 119880, https://doi.org/10.1016/j.energy.2021.119880.
[65] H. Li, S. Chen, D. Tang, Coal pore size distribution and adsorption capacity controlled by the coalification in china, Int. J. Hydrog. Energy 88 (2024) 594–603, https://doi.org/10.1016/j.ijhydene.2024.09.224.
[66] F.M. Valadi, M. Pasandideh-Nadamani, M. Rezaee, A. Torrik, M. Mirzaie, A. Torkian, Competitive adsorption of CO_2, N_2, and CH_4 in coal-derived asphaltenes, a computational study, Sci. Rep. 14 (2024), https://doi.org/10.1038/s41598-024-58347-6.